THE JOURNAL OF BIOLOGICAL CHEMISTRY
Vol. 272, No. 20, Issue of May 16, pp. 13270–13274, 1997
Printed in U.S.A.

Detection in Living Cells of Ca^{2+}-dependent Changes in the Fluorescence Emission of an Indicator Composed of Two Green Fluorescent Protein Variants Linked by a Calmodulin-binding Sequence

A NEW CLASS OF FLUORESCENT INDICATORS*

(Received for publication, February 19, 1997)

Valerie A. Romoser, Patricia M. Hinkle, and Anthony Persechini‡

From the Department of Pharmacology and Physiology, University of Rochester Medical Center, Rochester, New York 14642

We have designed a novel fluorescent indicator composed of two green fluorescent protein variants joined by the calmodulin-binding domain from smooth muscle myosin light chain kinase. When $(Ca^{2+})_4$-calmodulin is bound to the indicator (K_d = 0.4 nM), fluorescence resonance energy transfer between the two fluorophores is attenuated; the ratio of the fluorescence intensity measured at 505 nm to the intensity measured at 440 nm decreases 6-fold. Images of microinjected living cells demonstrate that emission ratios can be used to monitor spatio-temporal changes in the fluorescence of the indicator. Changes in indicator fluorescence in these cells are coupled with no discernible lag (<1 s) to changes in the cytosolic free Ca^{2+} ion concentration, ranging from below 50 nM to ~1 μM. This observation suggests that the activity of a calmodulin target with a typical 1 nM affinity for $(Ca^{2+})_4$-calmodulin is responsive to changes in the intracellular Ca^{2+} concentration over the physiological range. It is likely that the indicator we describe can be modified to detect the levels of ligands and proteins in the cell other than calmodulin.

The Ca^{2+}-binding protein calmodulin (CaM)[1] is a key transducer of intracellular Ca^{2+} ion signals, largely through its Ca^{2+}-dependent activation of many enzyme activities (1–4). Yet little is known about the extent and kinetics of enzyme activation *in vivo*, mainly because of the difficulty of directly monitoring target activation in the cell. Mitra *et al.* (5) have recently reported that changes in fluorescence resonance energy transfer (FRET) between variants of green fluorescent protein (GFP) can be used to monitor cleavage at a protease site within a linker amino acid sequence. We have designed a similar fluorescent indicator protein in which the GFP variants are linked by a CaM-binding sequence. This indicator exhibits a large CaM-dependent change in its fluorescence emission due to disruption of FRET when calmodulin is bound to the linker sequence. This response can be monitored in living cells, where it closely follows changes in the intracellular Ca^{2+} concentration.

MATERIALS AND METHODS

Expression and Purification of Proteins—The vector for expression of FIP-CB_{SM} is similar to the one described by Mitra *et al.* (5). The coding sequences for the BGFP (6) and RGFP (7) domains were produced by amplifying the GFP-encoding sequences in the BioBlue™ and BioYellow™ vectors obtained from PharMingen, Inc. (San Diego, CA). The vector pETIC, encoding a fluorescent indicator protein (FIP) control consisting of RGFP and BGFP domains joined by the linker sequence, GTSSGSSTGA, was generated first. The RGFP domain in pETIC is fused to the His_6-tag/thrombin/S-tag/enterokinase leader sequence derived from pET30a (Novagen, Inc., Madison, WI). The C terminus of the BGFP domain is fused to an additional His_6 sequence, also derived from pET30a. The vector pETIC-1 encodes FIP-CB_{SM}, which is identical to the FIP control, except that the linker has the sequence: GTS**SRRKWNKTGHAVRAIGRL**SSTGA. Boldface type denotes the CaM-binding sequence from avian smooth muscle myosin light chain kinase (8).

For expression, pETIC and pETIC-1 were transformed into *Escherichia coli* strain BL21(DE3). Cells containing pETIC or pETIC-1 were grown at 23 °C to an A_{600} of 0.6–0.8, and protein expression was induced by addition of isopropyl-1-thio-β-D-galactopyranoside to 0.5 mM. After incubating at 23 °C for ~40 h, cells were harvested. Control FIP and FIP-CB_{SM} were purified using His_6 affinity chromatography essentially as described by Mitra *et al.* (5). Vertebrate CaM expressed in *E. coli* was purified as described previously (9). The concentrations of control FIP and FIP-CB_{SM} were determined using an ϵ_{490} of 89 mM^{-1} cm^{-1}. Concentrations of FIP-CB_{SM} stock solutions were verified by titration with a standard CaM solution.

In Vitro Measurements of FIP-CB_{SM} Fluorescence—Fluorescence measurements were performed using a Photon Technology International (Monmouth Junction, NJ) QuantaMaster™ photon counting spectrofluorometer. Reaction volumes (3 ml) were incubated at 30 °C in a stirred cuvette. Excitation and emission slit widths were 5 nm. An excitation wavelength of 380 nm was used for *in vitro* measurements of FIP fluorescence. For most experiments, a buffer containing 25 mM Tris, 0.1 M NaCl, and 300 μM $CaCl_2$, pH 7.5, was used. For experiments in which the free Ca^{2+} ion concentration was varied, a buffer containing 50 mM Tris, 0.1 M NaCl, 0.5 mM $MgCl_2$, and 3 mM 1,2-bis(2-amino-5,5′-dibromophenoxy)ethane-*N,N,N′,N′*-tetraacetic acid, pH 7.5, was used. Aliquots of standard $CaCl_2$ solutions were added to achieve various levels of free Ca^{2+} ion, which were calculated using the MaxChelator program (10). The FIP-CB_{SM} fluorescence emission spectrum is essentially independent of the pH between 7.0 and 8.0, either in the presence or absence of bound $(Ca^{2+})_4$-CaM.

* This work was supported by United States Public Health Service Grant DK44322 (to A. P.), United States Public Health Service Grant DK19974 and Cancer Center Core Research Grant CA11198 (both to P. M. H.), and National Science Foundation Predoctoral Fellowship DGE9253919 (to V. A. R.). The costs of publication of this article were defrayed in part by the payment of page charges. This article must therefore be hereby marked "*advertisement*" in accordance with 18 U.S.C. Section 1734 solely to indicate this fact.

‡ To whom all correspondence should be addressed: Dept. of Pharmacology and Physiology, University of Rochester Medical Center, 601 Elmwood Ave., Box 711, Rochester, NY 14642. Tel.: 716-275-3087; Fax: 716-461-3259; E-mail: ajp2o@crocus.medicine.rochester.edu.

[1] The abbreviations used are: CaM, calmodulin; BAPTA, 1,2-bis(2-aminophenoxy)ethane-*N,N,N′,N′*-tetraacetic acid; TRH, thyrotropin-releasing hormone; FRET, fluorescence resonance energy transfer; GFP, green fluorescent protein; BGFP, blue-shifted GFP; RGFP, red-shifted GFP; FIP, fluorescent indicator protein; FIP-CB_{SM}, a fluorescent indicator protein in which BGFP and RGFP domains are joined by the CaM-binding domain from smooth muscle myosin light chain kinase.

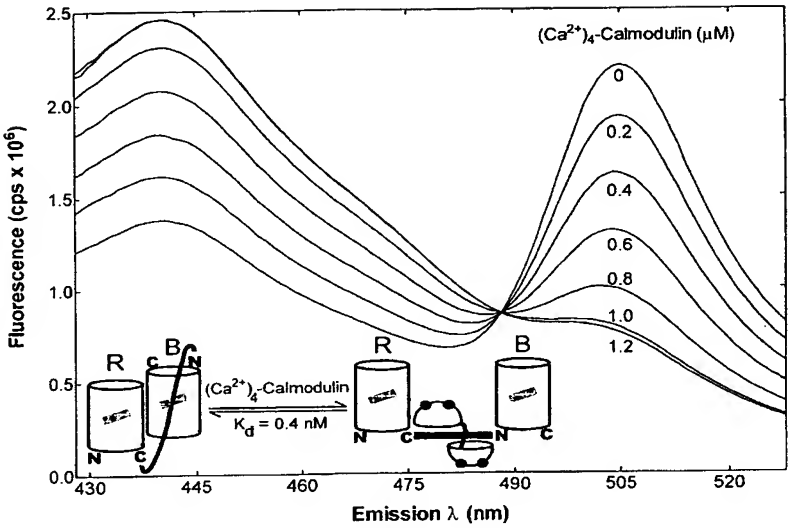

FIG. 1. **CaM-dependent changes in the FIP-CB_{SM} fluorescence emission spectrum.** FIP-CB_{SM} at a concentration of 1 μM was titrated with 0.2 μM increments of $(Ca^{2+})_4$-CaM. The effect of $(Ca^{2+})_4$-CaM on the FIP-CB_{SM} emission spectrum is completely reversed by adding 5 mM EDTA. A scheme depicting the conformational change undergone by FIP-CB_{SM} upon binding $(Ca^{2+})_4$-CaM is also presented in the figure. The RGFP (*R*) and BGFP (*B*) domains in FIP-CB_{SM} are joined by a linker sequence containing a CaM-binding domain. The fluorophores in the GFP domains are represented by *shaded rectangles*. The relative dimensions used for the GFP domains are based on the published crystal structures for GFP (14, 15). $(Ca^{2+})_4$-CaM is depicted as two hemispheres, corresponding to two EF hand pairs, joined by the flexible central helix. Ca^{2+} ions bound to the EF hands are depicted as *filled circles*.

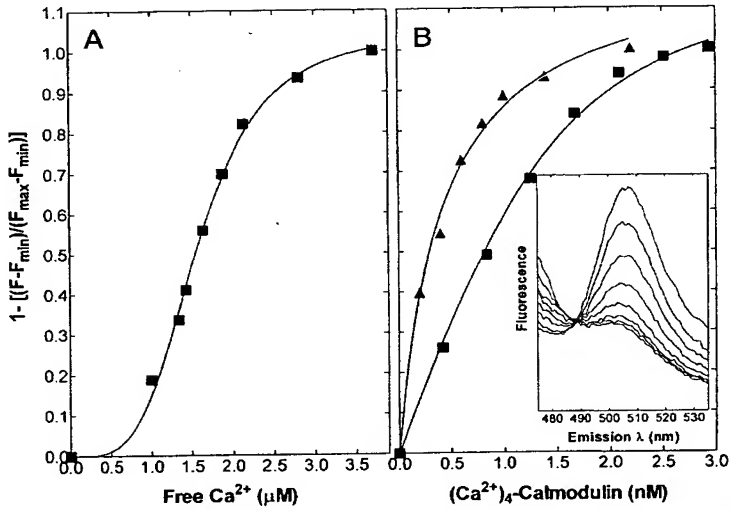

FIG. 2. **Characterization of CaM binding by FIP-CB_{SM}.** *A*, titration of a mixture of 8.2 nM FIP-CB_{SM} and 200 nM CaM with increasing concentrations of free Ca^{2+} ion. Data were fit to an equation of the form: $F = \alpha(L^n)/(L^n + K_a)$, where F is the fractional saturation of FIP-CB_{SM} with CaM, given in the figure as $1 - [(F - F_{min})/(F_{max} - F_{min})]$, L is the free Ca^{2+} ligand concentration, K_a is an apparent dissociation constant that depends upon the total amount of CaM, and n is the number of interacting sites, which equals 3.9 for the curve shown. This indicates that $(Ca^{2+})_4$-CaM is the species bound by FIP-CB_{SM}. F is the fluorescence measured at 505 nm, F_{max} and F_{min} are the values for F measured at maximal and minimal free Ca^{2+} ion concentrations, and α is a correction factor allowing adjustment of the maximal fraction of FIP-CB_{SM} bound to give the best fit. α values are between 1 and 1.1 for the curves shown in *panels A* and *B*. *B*, binding of $(Ca^{2+})_4$-CaM to FIP-CB_{SM} at concentrations of 1.4 (■) and 1.0 (▲) nM. The data measured at a 1 nM FIP-CB_{SM} concentration were fit to a standard single-site kinetic model as described previously (20). The data measured at a 1.4 nM FIP-CB_{SM} concentration were fit to an equation of the form: $F = \alpha\{(P_t + L_t + K_d) - [(P_t + L_t + K_d)^2 - 4(P_t)(L_t)]^{0.5}\}/2(P_t)$, where L_t is the total CaM concentration and P_t is the total FIP-CB_{SM} concentration. In both cases a K_d value of 0.4 nM was obtained. Emission spectra for titration of 1.4 nM FIP-CB_{SM} with $(Ca^{2+})_4$-CaM are shown in the *inset*.

Measurements of FIP-CB_{SM} Fluorescence in Cells—Human embryonic kidney cells (HEK-293) stably transfected with an epitope-tagged thyrotropin-releasing hormone (TRH) receptor (11) were grown on glass coverslips to 60–80% confluence, rinsed in Hank's balanced salt solution, and placed in a Sykes-Moore chamber maintained at 37 °C. Microinjections were performed on an Eppendorf Transjector 5246 equipped with a Micromanipulator 5171 using Femtotips from Eppendorf (Madison, WI). Microinjection solutions were centrifuged and filtered through 0.2-μm nitrocellulose filters and injected at pressures of 50–100 hectopascals for 0.1 s. Successful injections were visualized in brightfield and by observing at 530 nm the fluorescence of RGFP excited directly at 495 nm. After microinjection, cells were allowed to recover for at least 30 min.

Dynamic measurements were performed using a Dage CCD72 camera and Geniisys image intensifier system (Michigan City, IN) and IMAGE-1/AT analysis software from Universal Imaging (Media, PA). Fura-2 340/380 fluorescence excitation ratios were obtained as described previously (12). The fluorescence emission of FIP-CB_{SM} and control FIP excited at 380 nm was measured at 500-ms intervals using a 510-nm emission filter. Still photographs were obtained with a Cohu CCD camera (San Diego, CA) and a 440A integrator (Colorado Video, Inc., Boulder, CO) and analyzed with Metamorph software from Universal Imaging. Cells were illuminated at 380 nm, and emitted light was collected for 10–20 s at 510 nm and then at 440 nm.

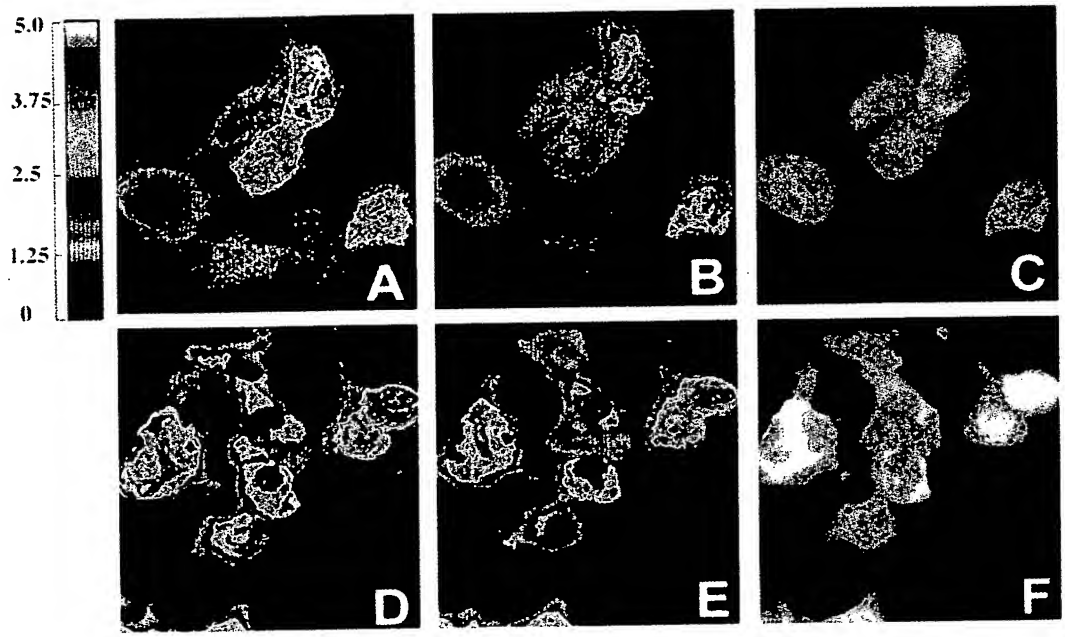

FIG. 3. **F_{510}/F_{440} emission ratio images of cells microinjected with FIP-CB_{SM}.** HEK-293 cells expressing the TRH receptor were microinjected with solutions containing 88 μM FIP-CB_{SM} and 88 μM CaM (*panels A–C*) or 85 μM FIP-CB_{SM} alone (*panels D–F*). *Panels A, B, D,* and *E* show in pseudocolor the F_{510}/F_{440} fluorescence emission ratios; the calibration bar depicts low (*bottom*) to high (*top*) fluorescence ratios. A scale relating pseudocolor values to relative numerical values is also shown in the figure. *Panels C* and *F* show the fluorescence emission of the cells seen in *panels A* and *B* or *D* and *E*, respectively, at basal $[Ca^{2+}]_i$ under 495 nm illumination, which directly excites the RGFP fluorophore in FIP-CB_{SM}. Cells were treated with 3 mM BAPTA (*panels A* and *D*), which reduces $[Ca^{2+}]_i$ to 30–50 nM, followed by 1 μM ionomycin + 10 mM $CaCl_2$ (*panels B* and *E*), which increases it to above 1 μM. The F_{510}/F_{440} fluorescence emission ratio decreases when $[Ca^{2+}]_i$ is increased, whether FIP-CB_{SM} is localized predominantly to the nucleus or to the cytoplasm. The F_{510}/F_{440} emission ratio decreases when $(Ca^{2+})_4$-CaM binds to FIP-CB_{SM} due to a reduction of FRET between the fluorophores in the RGFP and BGFP domains (Fig. 1).

RESULTS AND DISCUSSION

We have designed a fluorescent indicator protein containing two green fluorescent protein variants, with reported fluorescence excitation and emission maxima of 382 and 448 nm (BGFP) (6) and 495 and 509 nm (RGFP) (7), joined by an amino acid linker containing the CaM-binding sequence from smooth muscle myosin light chain kinase (8) (Fig. 1). We term this particular indicator FIP-CB_{SM}. Excitation of the fluorophore in the BGFP domain at 380 nm results in fluorescence emission at 505 nm from the fluorophore in the RGFP domain due to FRET between the fluorophores. FRET is essentially eliminated when FIP-CB_{SM} binds $(Ca^{2+})_4$-CaM, and the F_{505}/F_{440} ratio decreases from a value of 1.7 to a value of 0.3 (Fig. 1). FRET between the fluorophores in a control indicator protein lacking a CaM-binding sequence is not significantly affected by $(Ca^{2+})_4$-CaM. FIP-CB_{SM} binds $(Ca^{2+})_4$-CaM with a K_d of 0.4 nM, which is close to the 1 nM apparent K_d value for the complex between $(Ca^{2+})_4$-CaM and smooth muscle myosin light chain kinase (Fig. 2, *A* and *B*) (13).

Purified GFP dimerizes in solution, and crystallographic data suggest that the two GFPs are in an antiparallel orientation with the chromophores ~25 Å apart (14, 15). Molecular modeling indicates that the linker sequence between the GFP domains in FIP-CB_{SM} is long enough to allow them to interact in a similar manner. In the structures of the complexes between $(Ca^{2+})_4$-CaM and the CaM-binding sequences in several targets, including smooth muscle myosin light chain kinase, CaM enfolds the CaM-binding sequence forming a globular structure ~ 40 Å in diameter (16). Thus, when $(Ca^{2+})_4$-CaM binds to the linker in FIP-CB_{SM}, the inter-fluorophore distance is likely to be increased from ~25 Å to ~65 Å (Fig. 1). Since the efficiency of FRET is proportional to $1/r^6$, where r is the inter-fluorophore distance, this would explain the reduction in FRET observed when FIP-CB_{SM} binds (Ca^{2+})-CaM (17).

CaM-dependent changes in FRET between the fluorophores in FIP-CB_{SM} can be monitored in living cells, providing a view of free $(Ca^{2+})_4$-CaM levels in the cell. We have microinjected FIP-CB_{SM}, with or without equimolar CaM, into HEK-293 cells stably transfected with the $G_{q/11}$-coupled Ca^{2+}-mobilizing receptor for TRH. We estimate an intracellular FIP-CB_{SM} concentration in microinjected cells of 1–10 μM, similar to estimates for the intracellular concentrations of high-abundance CaM targets, such as smooth muscle myosin light chain kinase (18). Injection of FIP-CB_{SM} undoubtedly perturbs the balance between CaM and its targets. Coinjection of the indicator with equimolar CaM should help to restore it, but the exact mole ratio of CaM to its binding sites in the cell is unknown. The intracellular free Ca^{2+} ion concentration ($[Ca^{2+}]_i$) increases from below 50 nM, when cells are incubated in media containing BAPTA, to greater than 1 μM, when extracellular Ca^{2+} and ionomycin are added (data not shown). Corresponding fluorescence images show a clear Ca^{2+}-dependent reduction in the F_{510}/F_{440} ratios in cells injected either with FIP-CB_{SM} alone or with FIP-CB_{SM} and CaM. This indicates an increase in the fraction of FIP-CB_{SM} bound to $(Ca^{2+})_4$-CaM (Fig. 3). A greater reduction in the F_{510}/F_{440} ratio is evident in cells injected with both FIP-CB_{SM} and CaM. The basal fluorescence intensity of the RGFP acceptor (Fig. 3, *C* and *F*) is brighter in some regions of the cell than others due to the distribution of the probe within the cells. Some cells were injected in the nucleus, some into the cytoplasm, and some into both nuclear and cytoplasmic regions. FIP-CB_{SM} remained localized to the nucleus or cyto-

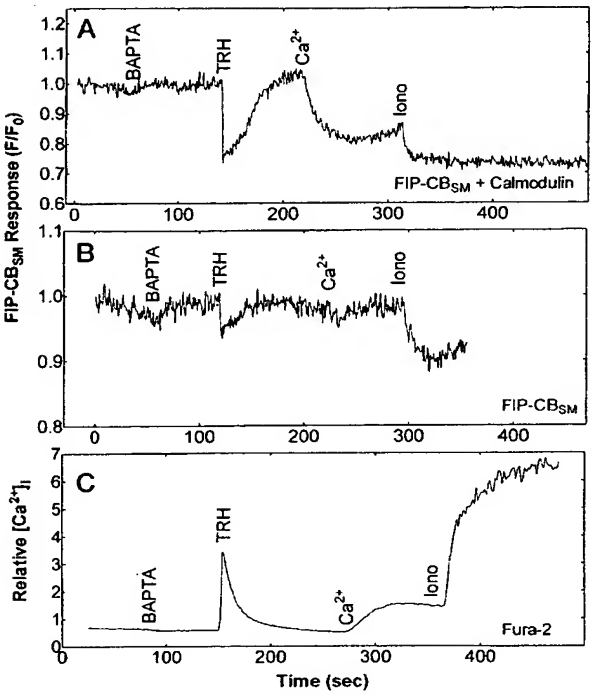

FIG. 4. **Kinetics of CaM activation in living cells.** Cells were microinjected with with solutions containing 88 μM FIP-CB_{SM} and 88 μM CaM (*panel A*), 88 μM FIP-CB_{SM} alone (*panel B*), or 2.5 mM Fura-2 free acid (*panel C*). At the indicated times, 3 mM BAPTA, 4 μM TRH, 5 mM $CaCl_2$, and 500 nM ionomycin were added to the bathing solution. Based on measurements in cell populations using Fura-2, BAPTA decreases $[Ca^{2+}]_i$ to below 50 nM, TRH increases it to 200–400 nM, and the combination of Ca^{2+} and ionomycin increase it to > 1 μM. *Panels A* and *B*, the average F_{510} emission intensity of 12–27 individual cells, expressed as F/F_0, with F_0 defined as the average of the first 10 values in the time course. The SEM for each time point averages 4%. Note the difference in scales for cells injected with equimolar FIP-CB_{SM} and CaM or FIP-CB_{SM} alone. *Panel C*, relative $[Ca^{2+}]_i$ values expressed as average Fura-2 340/380 excitation ratios. In control experiments, cells microinjected with a solution containing 88 μM control FIP, which lacks a CaM-binding sequence, either with or without equimolar CaM, show no detectable changes in F_{510} in response to externally applied BAPTA, TRH, $CaCl_2$, or ionomycin. Cells microinjected with Fura-2 free acid, and those injected with solutions containing Fura-2 + 88 μM CaM or Fura-2 + 88 μM CaM-binding peptide, show similar changes in Fura-2 fluorescence. The CaM-binding peptide used has the sequence: KRRWKKNFIAVSAANRFKK-amide, and is based on the CaM-binding domain in skeletal muscle myosin light chain kinase (21). The *axes* have been adjusted so that the times of TRH addition are aligned.

plasm in cells, depending upon its initial site of injection. The indicator, with a molecular mass of 63.4 kDa, would not be expected to move through nuclear pores, and such translocation was not observed. No systematic effort was made to compare the responses of the indicator in the nucleus and cytosol, although it is clear that similar responses occur in these compartments (Fig. 3). Ca^{2+}-dependent changes in the 510/440 emission ratio measured in cells suggest microheterogeneity in the response that may be artifactual, perhaps reflecting small changes in cell shape occurring during data collection. Investigations of a possible physiological basis for the apparent microheterogeneity are clearly a high priority.

To more precisely establish the kinetics and magnitude of the FIP-CB_{SM} response to changes in $[Ca^{2+}]_i$, the F_{510} of microinjected cells was measured at 500-ms intervals, while $[Ca^{2+}]_i$ was manipulated (Fig. 4). Reductions in F_{510} mirror increases in $[Ca^{2+}]_i$ caused by addition of TRH, Ca^{2+}, and ionomycin with no discernible lag (<1 s) (Fig. 4). Measurements using Fura-2 indicate that basal $[Ca^{2+}]_i$ in these cells is below 50 nM; it increases to 200–400 nM with TRH and to greater than 1 μM with the combination of external Ca^{2+} and ionomycin. In cells injected with equimolar FIP-CB_{SM} and CaM, the combination of Ca^{2+} and ionomycin causes a 30% reduction in F_{510}. This appears to represent the saturated response of the indicator, since it is reached and maintained when $[Ca^{2+}]_i$ is still increasing (Fig. 4*A*). Treatment of cells injected with FIP-CB_{SM} alone with TRH causes a ~6% reduction in F_{510}; the combination of Ca^{2+} and ionomycin causes a ~10% reduction (Fig. 4*B*). Thus, saturation of the FIP-CB_{SM} response is not approached in these cells, indicating that the CaM concentration is limiting.

The maximum fractional reduction in the F_{510} of FIP-CB_{SM} observed in cells was 30%, or about half of the maximal 65% CaM-dependent reduction in F_{510} measured *in vitro* (Fig. 1). Given the very different experimental systems used for measurements of fluorescence *in vitro* and *in vivo*, this difference in the maximal signals appears acceptable. The amount of probe injected was kept low to minimize perturbation of Ca^{2+}-CaM homeostasis. A consequence is that fluorescence filters with bandwidths of ~40 nm were required to obtain an adequate fluorescence signal. In contrast, the monochromator bandwidths used for *in vitro* measurements were about 3 nm. Some of the small discrepancy between *in vitro* and *in vivo* measurements of CaM-dependent changes in indicator fluorescence may therefore be attributable to the different optical systems used.

Our results clearly indicate that changes in $[Ca^{2+}]_i$ ranging from below 50 nM to ~1 μM are coupled to changes in the F_{510} of FIP-CB_{SM}. This suggests that the activity of a calmodulin target with a typical 1 nM affinity for $(Ca^{2+})_4$-calmodulin is responsive to changes in the intracellular Ca^{2+} concentration over the physiological range. It also suggests that physiological changes in $[Ca^{2+}]_i$ are coupled to changes in the free $(Ca^{2+})_4$-CaM concentration in the low nanomolar range. The free concentrations of $(Ca^{2+})_4$-CaM occurring in the cell are therefore ~1000-fold less than the total concentration of CaM (18). Thus, the calmodulin concentration in the cell is limiting; essentially all the $(Ca^{2+})_4$-CaM present in the cell must be bound to targets, as has been proposed based on studies of the intracellular mobility of tagged CaM (19). The very low physiological levels of free $(Ca^{2+})_4$-CaM indicate that small changes in the affinity of a typical target should significantly affect its level of activity at a submaximal $[Ca^{2+}]_i$, as recently demonstrated for smooth muscle myosin light chain kinase activity (18). The ability to monitor free $(Ca^{2+})_4$-CaM levels in living cells provides an exciting new approach for dissecting the processes that link variations in $[Ca^{2+}]_i$ to diverse cellular responses. Indeed, FIP-CB_{SM} appears to represent a new class of ligand-dependent indicators that have the potential of reporting the levels of a variety of proteins and other ligands in the cell, depending upon the nature of the linker sequence.

REFERENCES

1. Means, A. R., VanBerkum, M. F., Bagchi, I., Lu, K. P., and Rasmussen, C. D. (1991) *Pharmacol. Ther.* **50**, 255–270
2. Manalan, A. S., and Klee, C. B. (1984) *Adv. Cyclic Nucleotide Protein Phosphorylation Res.* **18**, 227–278
3. Lu, K. P., and Means, A. R. (1993) *Endocr. Rev.* **14**, 40–58
4. Vanaman, T. C., and Klee, C. B. (1982) *Adv. Protein Chem.* **35**, 213–321
5. Mitra, R. D., Silva, C. M., and Youvan, D. C. (1996) *Gene (Amst.)* **173**, 13–17
6. Heim, R., Prasher, D. C., and Tsien, R. Y. (1994) *Proc. Natl. Acad. Sci. U. S. A.* **91**, 12501–12504
7. Delegrave, S., Hawtin, R. E., Silva, C. M., Yang, M. M., and Youvan, D. C. (1995) *Bio/Technology* **13**, 151–154
8. Guerrero, V., Jr., Russo, M. A., Olson, N. J., Putkey, J. A., and Means, A. R. (1986) *Biochemistry* **25**, 8372–8381
9. Persechini, A., Blumenthal, D. K., Jarrett, H. W., Klee, C. B., Hardy, D. O., and

Kretsinger, R. H. (1989) *J. Biol. Chem.* **264,** 8052–8058
10. Bers, D., Patton, C., and Nuccitelli, R. (1994) *Methods Cell Biol.* **40,** 3–29
11. Yu, R., and Hinkle, P. M. (1997) *Mol. Pharmacol.*, in press
12. Nelson, E. J., and Hinkle, P. M. (1994) *Endocrinology* **135,** 1084–1092
13. Adelstein, R. S., and Klee, C. B. (1981) *J. Biol. Chem.* **256,** 7501–7509
14. Ormo, M., Cubitt, A. B., Kallio, K., Gross, L. A., Tsien, R. Y., and Remington, S. J. (1996) *Science* **273,** 1392–1395
15. Yang, F., Moss, L. G., and Phillips, G. N. (1996) *Nat. Biotechnol.* **14,** 1246–1251
16. Crivici, A., and Ikura, M. (1995) *Annu. Rev. Biophys. Biomol. Struct.* **24,** 85–116
17. Stryer, L. (1978) *Annu. Rev. Biochem.* **47,** 819–846
18. Tansey, M. G., Luby-Phelps, K., Kamm, K. E., and Stull, J. T. (1994) *J. Biol. Chem.* **269,** 9912–9920
19. Gough, A. H., and Taylor, D. L. (1993) *J. Cell Biol.* **121,** 1095–1107
20. Persechini, A., McMillan, K., and Leakey, P. (1994) *J. Biol. Chem.* **269,** 16148–16154
21. Blumenthal, D. K., and Krebs, E. G. (1987) *Methods Enzymol.* **139,** 115–126

Biochemistry **2001,** *40,* 2502−2510

Red Fluorescent Protein from *Discosoma* as a Fusion Tag and a Partner for Fluorescence Resonance Energy Transfer†

Hideaki Mizuno,‡ Asako Sawano,‡,§ Pharhad Eli,‡ Hiroshi Hama,‡ and Atsushi Miyawaki*,‡

Laboratory for Cell Function and Dynamics, Advanced Technology Development Center, Brain Science Institute, The Institute of Physical and Chemical Science (RIKEN), 2-1 Hirosawa, Wako-city, Saitama, 351-0198, Japan, and Brain Science Research Division, Brain Science and Life Technology Research Foundation, 1-28-12 Narimasu, Itabashi, Tokyo, 175-0094, Japan

Received September 26, 2000; Revised Manuscript Received November 28, 2000

ABSTRACT: The biochemical and biophysical properties of a red fluorescent protein from a *Discosoma* species (DsRed) were investigated. The recombinant DsRed expressed in *E. coli* showed a complex absorption spectrum that peaked at 277, 335, 487, 530, and 558 nm. Excitation at each of the absorption peaks produced a main emission peak at 583 nm, whereas a subsidiary emission peak at 500 nm appeared with excitation only at 277 or 487 nm. Incubation of *E. coli* or the protein at 37 °C facilitated the maturation of DsRed, resulting in the loss of the 500-nm peak and the enhancement of the 583-nm peak. In contrast, the 500-nm peak predominated in a mutant DsRed containing two amino acid substitutions (Y120H/K168R). Light-scattering analysis revealed that DsRed proteins expressed in *E. coli* and HeLa cells form a stable tetramer complex. DsRed in HeLa cells grown at 37 °C emitted predominantly at 583 nm. The red fluorescence was imaged using a two-photon laser (Nd:YLF, 1047 nm) as well as a one-photon laser (He:Ne, 543.5 nm). When fused to calmodulin, the red fluorescence produced an aggregation pattern only in the cytosol, which does not reflect the distribution of calmodulin. Despite the above spectral and structural complexity, fluorescence resonance energy transfer (FRET) between *Aequorea* green fluorescent protein (GFP) variants and DsRed was achieved. Dynamic changes in cytosolic free Ca^{2+} concentrations were observed with red cameleons containing yellow fluorescent protein (YFP), cyan fluorescent protein (CFP), or Sapphire as the donor and RFP as the acceptor, using conventional microscopy and one- or two-photon excitation laser scanning microscopy. Particularly, the use of the Sapphire−DsRed pair rendered the red cameleon tolerant of acidosis occurring in hippocampal neurons, because both Sapphire and DsRed are extremely pH-resistant.

Green fluorescent proteins (GFPs)[1] are found in a large number of bioluminescent coelenterates (*1*). GFPs were thought to be an accessory emitter protein of the cnidarian luminescent system, deriving their excitation by nonradiative energy transfer in association with the luciferase reaction. The GFP from *Aequores victoria* (*Aequorea* GFP) is now widely used in molecular and cellular biology studies (*2*). However, several GFP-like fluorescent proteins have been isolated from fluorescent but nonbioluminescent Anthozoa species (*3*). Among them is a red-emitter peaking at 583 nm, called DsRed or drFP583. Although the GFP-like fluorescent proteins have only 26−30% sequence identity with *Aequorea* GFP, several features of GFP structure are probably conserved, including the "β-can" fold.

Since DsRed has longer wavelengths of excitation and emission than are currently available from *Aequorea* GFP, it would be useful for multi labels and reporters and could serve as a resonance energy transfer acceptor. However, complicated features in its spectra and structure have been pointed out, which limit the usefulness of DsRed as a tool. First, the absorption spectrum of DsRed is broad with several shoulders and peaks other than the main peak at 558 nm. Also, a small peak at 500 nm in the emission spectrum is mentioned in the manufacturer's brochure (Clontech). Second, a spotty pattern of red fluorescence has often been observed when DsRed was fused to a certain protein and expressed in eukaryotic cells, suggesting aggregation of the chimera protein.

Spectral and structural features of fluorescent proteins are generally dependent on each other. With the exception of *Aequorea* GFP, all GFP molecules so far studied have been

† This work was partly supported by grants from CREST of JST (Japan Science and Technology) and the Japanese Ministry of Education, Science and Culture.

* To whom correspondence should be addressed at the Laboratory for Cell Function and Dynamics, Advanced Technology Development Center, Brain Science Institute, The Institute of Physical and Chemical Science (RIKEN); 2-1 Hirosawa, Wako-city, Saitama, 351-0198, Japan. Tel +81-48-467-5917; Fax +81-48-467-5924; E-mail matsushi@brain.riken.go.jp.

‡ The Institute of Physical and Chemical Science (RIKEN).

§ Brain Science and Life Technology Research Foundation.

[1] Abbreviations: $[Ca^{2+}]_c$, calcium concentration in the cytosol; CaM, calmodulin; CBB, Coomassie brilliant blue R250; CFP, cyan fluorescent protein; CRC2, cyan red cameleon-2; DsRed, red fluorescent protein cloned from *Discosoma* coral; DTT, dithiothreitol; ECFP, enhanced cyan fluorescent protein; EYFP-V68L/Q69K, enhanced yellow fluorescent protein that is less pH-sensitive; FRET, fluorescence resonance energy transfer; GFP, green fluorescent protein; IPTG, isopropyl-β-D-thiogalactopyranoside; MALS, multi-angle light scattering; RT, room temperature; Sapphire, ≡H9-40 which has mutations S72A/Y145F/T203I; SapRC2, Sapphire red cameleon-2; SDS−PAGE, sodium dodecyl sulfate−polyacrylamide gel electrophoresis; TTX, tetrodotoxin; YFP, yellow fluorescent protein; YRC2, yellow red cameleon-2.

10.1021/bi002263b CCC: $20.00
Published on Web 02/01/2001

stable nondissociable dimers in diluted aqueous solution (*4*). In contrast, *Aequorea* GFP forms a dimeric complex but only at a high protein concentration. It is of interest that wild-type *Aequorea* GFP undergoes large changes in its absorption spectrum upon dimerization (*5*). In the present study, we investigated the inter-relationships between the structure and spectra of DsRed in hopes of achieving better use of the fluorescent protein as a fusion tag and a partner for fluorescence resonance energy transfer (FRET).

Cameleons are chimeric proteins consisting of a blue or cyan mutant of GFP, calmodulin (CaM), a glycylglycine linker, the CaM binding peptide of myosin light chain kinase (M13), and a green or yellow version of GFP (*6*). Ca^{2+} binding to the CaM causes intramolecular CaM binding to M13. The resulting change from an extended to a more compact conformation increases the efficiency of FRET between the shorter to the longer wavelength mutant GFP. To obtain adequate expression and brightness of the mutant GFPs in mammalian cells, enhanced genes with mammalian codon usage and mutations for improved folding at 37 °C were developed. Also the blue mutant (BFP) proved to be the dimmest and most bleachable of the GFPs. It also required ultraviolet excitation, which is potentially injurious, excites the most cellular autofluorescence, and could interfere with the use of caged compounds. Therefore, enhanced cyan and yellow mutants, ECFP and EYFP, have been substituted for the original blue and green mutants, respectively, to make "yellow cameleons". Despite the considerable promise of yellow cameleons, they still have problems that need amelioration. One of the problems is that EYFP is quenched by acidification. This problem perturbed the signals of yellow cameleons, mimicking a decrease in $[Ca^{2+}]$ when the cellular environment acidified. The pH-sensitivity of yellow cameleons has been greatly reduced by introducing mutations V68L and Q69K into EYFP (EYFP-V68L/Q69K) (*7*). The improved yellow cameleons, including yellow cameleon-2.1, permit Ca^{2+} measurements without perturbation by pH changes from 6.5 to 8.0. Mutations have been also introduced into the Ca^{2+} binding loops of CaM to tune the affinity of yellow cameleons for Ca^{2+}. Herein, we experimented with three pairs: YFP−DsRed, CFP−DsRed, and Sapphire−DsRed for cameleons [Sapphire is a GFP variant (≡H9-40) containing a mutation of Thr203 to Ile, which results in a stabilization of the neutral form of the chromophore (*8*)]. Features of the resulting "yellow-red cameleons", "cyan-red cameleons", and "Sapphire-red cameleons" will be discussed.

EXPERIMENTAL PROCEDURES

Recombinant DsRed Expressed in E. coli. The gene for DsRed was amplified by polymerase chain reaction (PCR) using pDsRed1-1 (Clontech) as a template with a forward primer containing a *Bam*HI site and a reverse primer containing an *Eco*RI site. The restricted product was cloned in-frame into the *Bam*HI/*Eco*RI sites of $pRSET_B$ (Invitrogen). The resulting plasmid DNA, $DsRed/pREST_B$, encoded DsRed with an Xpress tag at the N-terminus. DsRed-mu43 was obtained by PCR-based random mutagenesis (*9*). Expression of the recombinant DsRed in *E. coli* and its purification were carried out as previously reported (*3*, *10*). The temperature and time of incubation after addition of isopropyl-β-D-thiogalactopyranoside (IPTG) were changed for optimization of the expression. Purity of the protein sample was checked by sodium dodecyl sulfate−polyacrylamide gel electrophoresis (SDS−PAGE) followed by Coomassie brilliant blue R250 (CBB) staining. Protein concentration was determined using a protein assay kit (Bio-Rad) using bovine serum albumin (BSA) as a standard. Absorption, emission, and excitation spectra were acquired in 50 mM HEPES, pH 8, using a U3310 spectrophotometer (Hitachi, Tokyo, Japan) and a F2500 fluorescence spectrophotometer (Hitachi). For size-exclusion chromatography, Superdex 200HR10/30 (Amersham Pharmacia) was installed on ÄKTA explorer 10S (Amersham Pharmacia), and fluorescence was monitored with an RF-10AXL fluorescence detector (Shimadzu, Kyoto, Japan). The Xpress tag was liberated from DsRed expressed in *E. coli* by incubation with recombinant enterokinase (2 units/100 μg of protein, Novagen), at 20 °C for 20 h. Multi-angle light scattering (MALS) was measured with a multi-angle light photometer (DAWN, Wyatt, Santa Barbara, CA) connected to a Shodex HPLC system (Showa Denko, Tokyo, Japan) on which size-exclusion columns (tandem connection of KW-804 and KW-803, Showa Denko) were installed (*11*).

Expression of DsRed in HeLa Cells. The DsRed gene was amplified by PCR with a sense primer containing a *Hin*dIII site and kozak consensus sequence (TCCACCATG), and a reverse primer containing an *Eco*RI site. The restricted fragment was inserted into the *Hin*dIII/*Eco*RI sites of pcDNA3 (Invitrogen) to construct DsRed/pcDNA3. HeLa cells were grown on a 10-cm tissue culture dish to 40% confluence in Dulbecco's modified Eagle's medium (Sigma) with 10% fetal bovine serum (Sigma), and transfected with 4 μg/dish of DsRed/pcDNA3 using lipofectin (GIBCO). One to three days after the transfection, the dish was placed on ice for 10 min, and then cells were washed twice in 10 mL of phosphate-buffered saline. Cell extract was prepared by incubating cells for 5 min on ice in 500 μL of lysis buffer (1% Triton X-100, 50 mM HEPES−NaOH, pH 8.0) supplemented with 50 μM phenylmethylsulfonyl fluoride, 10 μM leupeptin, 10 μM E-64, and 1 μM pepstatin A. The lysate was used for size-exclusion chromatography. Eluate was fractionated and subjected to SDS−PAGE followed by immunoblotting. DsRed on a membrane was detected using a living colors D.s. peptide antibody (Clontech) and an ECL detection system (Amersham Pharmacia).

Acquisition of Fluorescence Images of HeLa Cells Expressing ECFP and DsRed with Two-Photon Excitation Laser Scanning Microscopy. HeLa cells were grown on a 35-mm glass-bottom dish and cotransfected with 1 μg/dish of DsRed/pcDNA3 and ECFP/pcDNA3. ECFP−CaM/pcDNA3 was described previously (*6*). The gene for full-length DsRed was amplified by PCR, and was substituted for the ECFP gene to create DsRed−CaM/pcDNA3. Cells were observed with a two-photon laser scanning microscope based on a Fluoview FV500 scanning unit (Olympus, Tokyo, Japan) and two pulse lasers: a Ti:sapphire laser (Tsunami; Spectra Physics, Mountain View, CA) and an Nd:YLF laser (DPM-1000PC; Coherent Scotland, Glasgow, Scotland). The objective lens used was UPlanAPO 60xW/IR (Olympus). ECFP and DsRed were excited at 800 nm with the Ti: sapphire laser and at 1047 nm with the Nd:YLF laser, respectively. Excitation beams from the two lasers were alternately irradiated to the sample. Fluorescence was detected through band-pass filters BA465-495 (Olympus) and

Table 1: Filters and Dichroic Mirrors Used To Acquire Images of Neurons Expressing Red Cameleons with Conventional Fluorescence Microscopy[a]

	YRC2	CRC2	SapRC2
Ex. filter	480DF10	440DF20	400DF15
dichroic mirror	505DRLP	455DRLP	455DRLP
Em. filter, donor	535DF25	480DF30	510WB40
Em. filter, acceptor	565EFLP	565EFLP	565EFLP

[a] All filters and mirrors were purchased from Omega.

Table 2: Lasers, Filters, and Dichroic Mirrors Used To Acquire Images of HeLa Cells Expressing Red Cameleons with Laser Scanning Microscopy

	YRC2	CRC2	SapRC2
Ex. wavelength	488 nm[a]	800 nm[b]	770 nm[b]
dichroic mirror	DM351/488[c]	RDM650[c] & DM650[c]	RDM650[c] & DM650[c]
IR cut filter		BA650RIF[c]	BA650RIF[c]
beam splitter	SDM560[c]	DM505[c]	560DRLP
Em. filter, donor	BA515-550[c]	BA465-495[c]	510WB40
Em. filter, acceptor	BA560IF[c]	590DF35	580DF30

[a] Argon-ion laser (Omnichrome, Melles Griot). [b] Ti: sapphire laser (Tsunami, Spectra Physics). [c] Filters and mirrors obtained from Olympus. Others were from Omega.

590DF35 (Omega) for ECFP and DsRed, respectively. ECFP and DsRed fused to CaM were observed using the same instruments.

Dissociation Culture of Hippocampal Neurons. Primary neurons were prepared from Wistar rat embryos (E17-18) according to references (*12*, *13*). Calcium phosphate precipitation was used to transfect the neurons (*14*).

Calcium Imaging Using Red Cameleons. The cDNAs of all red cameleons were constructed from the cDNA of yellow cameleon-2.1, one of the improved yellow cameleons that have EYFP-V68L/Q69K. CRC2 (cyan red cameleon-2) was made by substituting DsRed for EYFP-V68L/Q69K. In addition to the substitution, replacement of ECFP with EYFP-V68L/Q69K and Sapphire produced YRC2 (yellow red cameleon-2) and SapRC2 (Sapphire red cameleon-2), respectively. HeLa cells and hippocampal neurons were transfected with mammalian expression vectors containing the genes for YRC2, CRC2, and SapRC2. They were imaged using the optical apparatus described in Table 1 (conventional microscopy) and Table 2 (one- or two-photon excitation laser scanning microscopy). The conventional microscopy system had a 75-W xenon lamp, an inverted microscope (IX 70, Olympus), a cooled CCD camera (MicroMax, Roper Scientific), and a filter changer (Lambda 10-2, Sutter Instruments) to alternate two emission filters for dual-emission ratio imaging. These instruments were controlled by MetaFluor 4.0 software (Universal Imaging).

RESULTS

Expression of DsRed in E. coli, and the Absorption and Emission Spectra. DsRed fused with Xpress tag (Invitrogen) at the N-terminus was expressed in *E. coli*. The tag contains six histidines followed by an enterokinase cleavage site; its molecular mass is 3.5 kDa. The temperature and time of *E. coli* incubation after addition of IPTG were optimized for efficient production of DsRed. Four different conditions [at room temperature (RT) or 37 °C, for 24 or 75 h] are listed in Table 3. DsRed was recovered from the medium as well as the cell lysate, since the fluorescence appeared also in the culture medium except at RT for 24 h, suggesting a warmer temperature to facilitate secretion of DsRed into the medium. DsRed with the tag was purified with a Ni−NTA column to a single band on SDS−PAGE (data not shown). We found that longer incubation at a warmer temperature yielded more red fluorescence in both bacteria and the medium. By contrast, *Aequorea* GFP is more abundantly expressed at lower temperatures and accumulates inside cells; incubation at RT for 24 h should usually yield sufficient production of *Aequorea* GFP.

Table 3: Expression of DsRed in *E. coli*

sample	condition after IPTG addition: temp	time (h)	prepared from	amount of DsRed (mg/100 mL of culture)	F_{500}/F_{580} (%)
$DsRed_{RT,24,p}$	RT	24	cells	9	61
$DsRed_{RT,75,p}$	RT	75	cells	4	13
$DsRed_{RT,75,s}$	RT	75	supernatant	15	9
$DsRed_{37,24,p}$	37 °C	24	cells	13	14
$DsRed_{37,24,s}$	37 °C	24	supernatant	6	12
$DsRed_{37,75,p}$	37 °C	75	cells	4	6
$DsRed_{37,75,s}$	37 °C	75	supernatant	24	5

Figure 1A shows absorption and emission spectra of $DsRed_{RT,24,p}$. The absorption spectrum was broad with five peaks at wavelengths of 277, 335, 487, 530, and 558 nm. It differed slightly from that reported by Matz et al. (*3*); the 277-nm and 487-nm peaks showed relatively higher amplitudes in the spectrum of $DsRed_{RT,24,p}$ than in the spectrum previously reported (*3*). Since the absorbance at 277 nm represents the quantity of the purified protein, it suggested that the chromophore was less formed in the $DsRed_{RT,24,p}$ sample. Next, the emission spectrum of $DsRed_{RT,24,p}$ was obtained by excitation at the wavelength of each of the absorption peaks. When excited at 558, 530, or 335 nm, a peak appeared at 583 nm on the emission spectrum. In contrast, excitation of the protein sample at 487 or 277 nm gave rise to a minor peak at 500 nm in addition to the 583-nm peak.

We noticed that a larger amount of red fluorescence was produced by incubated cells at a higher temperature and for a longer period. We suspected that better expression of DsRed resulted in a different spectral property. Therefore, we examined the spectra of $DsRed_{37,75,s}$ (Figure 1B). The absorption spectrum corresponded well with that reported by Matz et al. (*3*). The 277-nm and 487-nm peaks were less significant in $DsRed_{37,75,s}$ than in $DsRed_{RT,24,p}$. Again, the emission spectra of $DsRed_{37,75,s}$ were obtained by excitation at the absorption peaks. The minor peak at 500 nm was essentially missing, when $DsRed_{37,75,s}$ was excited at 277 and 487 nm. These results suggested the presence of a subcomponent of fluorescence, which was excited at 277 and 487 nm and emitted at 500 nm, and which resided transiently in DsRed during its maturation.

Figure 1D and 1E show the excitation spectra of $DsRed_{RT,24,p}$ and $DsRed_{37,75,s}$, respectively, with an emission wavelength of 583 nm. Also the excitation spectrum of $DsRed_{RT,24,p}$ with the emission at 500 nm is shown in Figure 1D; there were two excitation peaks around 280 and 460 nm. Excitation of $DsRed_{RT,24,p}$ at 460 nm gave both the major (583 nm) and the minor (500 nm) emission peaks. The ratio of peak

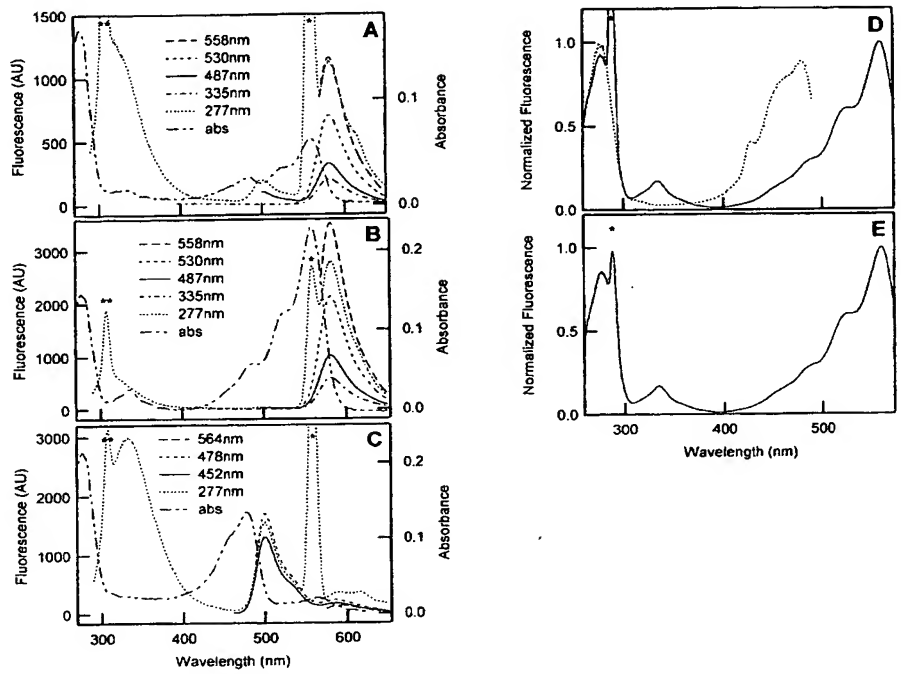

FIGURE 1: (A−C) Absorption and emission spectra of $DsRed_{RT,24,p}$ (A), $DsRed_{37,75,s}$ (B), and DsRed-mu43 (C). The emission spectra were obtained with excitation at the wavelengths denoted. (D and E) Excitation spectra of $DsRed_{RT,24,p}$ (D) and $DsRed_{37,75,s}$ (E) acquired with emission wavelengths of 583 nm (solid line) and 500 nm (D, dotted line). Excitation spectra were normalized with the highest value of the respective spectra. The Raman peaks from water are indicated by **, and the peaks due to scattering of the excitation light by *.

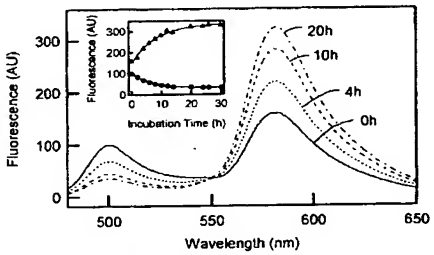

FIGURE 2: Time-dependent changes in emission spectra of $DsRed_{RT,24,p}$ by incubation at 37 °C. Emission spectra were obtained by excitation at 460 nm. Inset: Peak heights at 500 (circles) and 580 (triangles) nm on the spectra are plotted against incubation time. They were fitted with exponential curves, and τ values were estimated to be 6.3 and 8.4 h, respectively.

amplitudes at 500 to 583 nm ($R_{500/583}$) was low when DsRed was produced at 37 °C and for 75 h, and was prepared from the medium. Assuming that there is a transition from the subcomponent emitting at 500 nm to the main component at 583 nm during maturation of DsRed, we attempted to mature $DsRed_{RT,24,p}$. Incubation of $DsRed_{RT,24,p}$ at 37 °C resulted in a 68% reduction of the 500-nm peak with a 107% increase in the 583-nm peak, and thus $R_{500/583}$ decreased from 61% to 10% (Figure 2). The temporal profiles of the decrease and increase were fitted with exponential curves with similar τ values: 6.3 and 8.4 h, respectively (Figure 2, inset). In addition, all of the spectra passed through an isosbestic point (Figure 2). These results suggested a simple two-state mechanism for the transition.

The presence of the subcomponent was further verified by obtaining a mutant DsRed (DsRed-mu43) which emitted principally at 500 nm. DsRed-mu43 carried two amino acid substitutions (Y120H/K168R). DsRed-mu43 absorbed at 277, 452, 478, and 564 nm (Figure 1C), but not around 335 nm. Excitation at each of the absorption peaks gave the 500-nm peak and a tiny emission peak around 600 nm. In contrast to wild-type DsRed, incubation at 37 °C did not shift the emission spectrum to a longer wavelength (data not shown).

Wild-type *Aequorea* GFP has a bimodal excitation spectrum with peaks at 395 and 475 nm. Underlying the two maxima are protonated and deprotonated states of Tyr66, which forms part of the chromophore (2). Because the corresponding amino acid of the chromophore-forming triad in DsRed is also a tyrosine residue, we examined the pH-sensitivity of DsRed. Emission of $DsRed_{37,75,s}$ at 583 nm was stable between pH 5 and 11 (Figure 3). $R_{500/583}$ was not altered either when the emission spectra of $DsRed_{RT,24,p}$ were measured at various pHs.

Size-Exclusion Chromatography for DsRed Expressed in E. coli. $DsRed_{RT,24,p}$ was applied to Superdex 200, a size-exclusion column (Amersham Pharmacia), and chromatograms were acquired by monitoring the absorption at 280 nm (A_{280}) for total protein, the absorption at 560 nm (A_{560}), and the fluorescence at 580 nm with excitation at 560 nm ($F_{580/560}$) for the main fluorescence component. A single peak at 13.9 mL was detected on all three traces (Figure 4A). The same chromatogram was obtained using $DsRed_{37,75,s}$ and DsRed-mu43 (data not shown). The fluorescence spectra of the peak fraction in Figure 4A and of $DsRed_{RT,24,p}$ were compared (Figure 4A, inset). The comparison indicated the

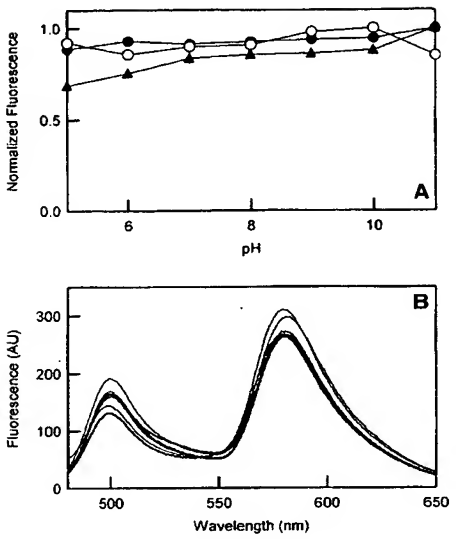

FIGURE 3: pH-dependency of the fluorescence of DsRed. (A) Emission intensities at 583 nm with excitation at 558 nm for $DsRed_{37,75,s}$ (open circles) and $DsRed_{RT,24,p}$ (closed circles), and emission intensities at 500 nm with excitation at 460 nm for $DsRed_{RT,24,p}$ (closed triangles) were measured at various pHs. Data were normalized with the highest values of respective samples. (B) Emission spectra of $DsRed_{RT,24,p}$ at various pHs obtained by excitation at 460 nm. Buffers used were phosphate (pH 11), glycine–NaOH (pH 10, 9), HEPES–NaOH (pH 8), MOPS–NaOH (pH 7), MES–NaOH (pH 6), and sodium acetate (pH 5).

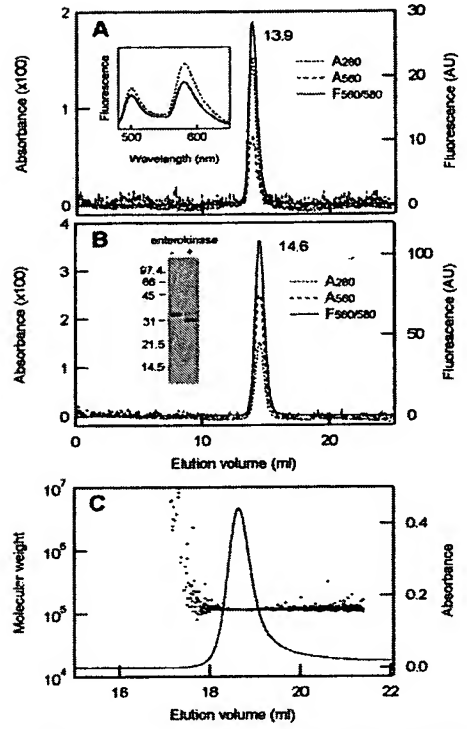

FIGURE 4: Size-exclusion chromatography of DsRed. $DsRed_{RT,24,p}$ (A) and enterokinase-treated $DsRed_{37,75,s}$ (B) were applied onto Superdex 200, and chromatograms were obtained by monitoring A_{280}, A_{560}, and $F_{560/580}$. The inset in (A) shows emission spectra of $DsRed_{RT,24,p}$ (dotted line) and of the fraction corresponding to the 13.9-mL peak (solid line), acquired with excitation at 460 nm. The inset in (B) shows band patterns of $DsRed_{37,75,s}$ before and after the enterokinase treatment on SDS–PAGE followed by CBB staining. (C) Determination of the absolute molecular weight of the enterokinase-treated $DsRed_{37,75,s}$. The molecular weight was calculated from data of MALS and overlaid on the chromatogram of A_{280}.

main component and subcomponent not to be separable from each other by hydrodynamic behavior. We treated $DsRed_{37,75,s}$ with enterokinase to remove the Xpress tag, which might contribute to complex formation. Liberation of the tag was confirmed by SDS–PAGE followed by CBB staining (Figure 4B, inset). The tag-free DsRed was eluted at 14.6 mL (Figure 4B), and its apparent molecular mass was estimated to be 75.6 kDa.

Next, we determined the absolute molecular mass of $DsRed_{37,75,s}$ using a multiangle light scattering analysis. We applied the enterokinase-treated sample onto two size-exclusion columns that were tandemly connected (KW-804 and KW-803, Shodex), and analyzed the eluate using a multiangle laser light scattering photometer (Figure 4C). The absolute molecular mass was calculated to be 114.7 kDa. This value was 4.37 times larger than that (26.24 kDa) deduced from the primary structure of the enterokinase-treated DsRed. It was therefore concluded that the DsRed expressed in bacteria forms a homotetrameric complex. Since the same elution pattern was obtained with $DsRed_{RT,24,p}$ and DsRed-mu43 as well as $DsRed_{37,75,s}$, and even when the samples were diluted to 3.3 nM, the tetramer complex should be stable, irrespective of the fluorescence property or maturation state.

Expression of DsRed in Mammalian Cells. Based on the temperature-dependent maturation of DsRed, we speculated that the maturation of red fluorescence might proceed efficiently in mammalian cells, which are usually kept at 37 °C. First, we studied how soon the fluorescence appeared in cell extracts from HeLa cells that had been transfected with DsRed/pcDNA3. Figure 5A shows emission spectra of the cell extracts prepared 24, 48, and 72 h after transfection, which were excited at 460 and 558 nm. The main component (emission around 583 nm) emerged between 24 and 48 h after transfection, while the subcomponent (emission around 500 nm) was undetectable. The extract at 72 h post-transfection was subjected to size-exclusion chromatography with monitoring of $F_{560/580}$ (Figure 5B). Eluates were fractioned and subjected to immunoblotting analysis using an anti-DsRed antibody. Although three peaks (8.1, 14.7, and 21.8 mL) were seen on the chromatogram, only the peak at 14.7 mL was shown to contain DsRed. This position was similar to that (14.6 mL) of the bacterially expressed DsRed that was treated with enterokinase.

HeLa cells were cotransfected with DsRed/pcDNA3 and ECFP/pcDNA3. The fluorescence was observed using two-photon excitation microscopy with a 1047-nm pulse laser (Coherent) for DsRed and with an 800-nm pulse laser (Tsunami) for ECFP (Figure 6A,B). Although both DsRed and ECFP were apparently distributed throughout the cells, there was a slight difference in that the red fluorescence was observed evenly in the cytosol and nucleus, whereas the cyan fluorescence was slightly concentrated in the nucleus. When fused to calmodulin (CaM), the difference in distribution

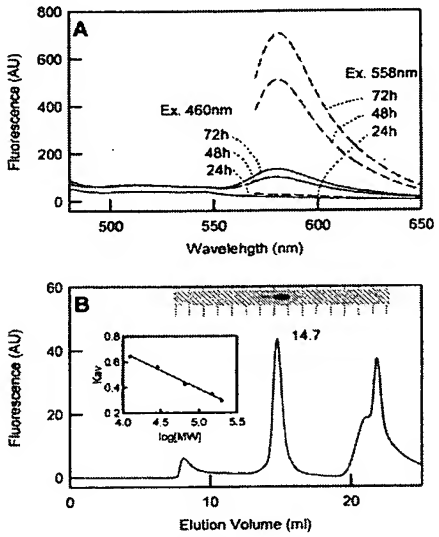

FIGURE 5: Emission spectra and size-exclusion chromatograms of DsRed expressed in HeLa cells. (A) Cell extracts were prepared 24, 48, and 72 h after transfection, and their emission spectra were acquired with excitation at 460 and 558 nm. (B) The cell extract prepared after 72 h transfection was applied onto Superdex 200, and the red fluorescence was monitored ($F_{560/580}$). The fractions were immunoblotted using anti-DsRed antibody. (B, inset) Calibration curve for the size-exclusion chromatography. Standards used are β-amylase (200 kDa), alcohol dehydrogenase (150 kDa), albumin (66 kDa), carbonic anhydrase (29 kDa), and cytochrome *c* (12.4 kDa).

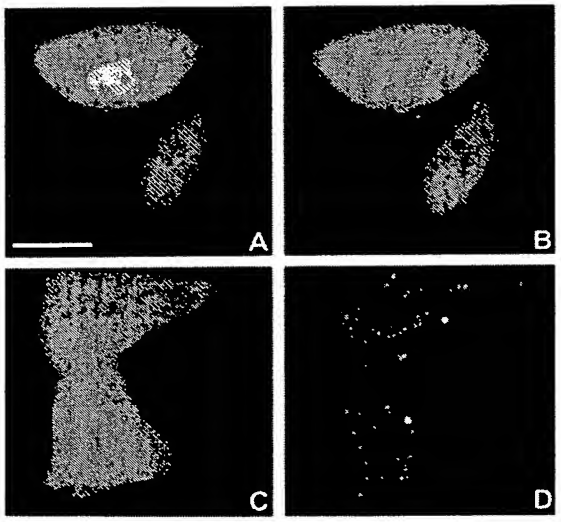

FIGURE 6: Distribution of DsRed and DsRed−CaM expressed in HeLa cells. Cells coexpressing ECFP and DsRed (A, B) or ECFP−CaM and DsRed−CaM (C, D) were imaged using a laser scanning microscope. Excitation beams for ECFP (800 nm, Ti:sapphire laser) and DsRed (1047 nm, Nb:YLF laser) were alternately irradiated. Images for ECFP were acquired through BA465-495 (A, C) and for DsRed through 590DF35 (B, D). The bar shown in (A) indicates 20 μm.

between DsRed and ECFP was remarkable (Figure 6C,D). Regardless of CaM, the same distribution of cyan fluorescence was observed. By contrast, the fluorescence of

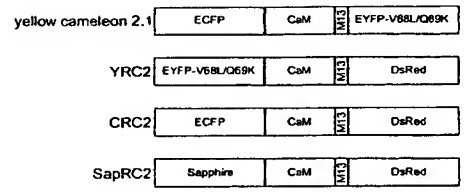

FIGURE 7: Schematic structures of yellow cameleon-2.1, YRC2, CRC2, and SapRC2.

DsRed−CaM showed many spots scattered over the cytosol, suggesting aggregation of the chimera proteins.

Expression of Red Cameleons in HeLa Cells. Three red cameleons were constructed (Figure 7): yellow red cameleon-2 (YRC2), cyan red cameleon-2 (CRC2), and Sapphire red cameleon-2 (SapRC2). These camelons contained DsRed as the acceptor and EYFP-V68L/Q69K, ECFP, and Sapphire, respectively, as the donor. All the red cameleons had intact CaMs, and thus exhibited a relatively high affinity for Ca^{2+} (K'_d = 0.2−0.4 μM; data not shown). We expressed the red cameleons in HeLa cells and obtained sectional images of $[Ca^{2+}]_c$. Selective excitation of the donor GFP over the acceptor DsRed was attempted using a 488-nm beam argon laser for YRC2 and using a mode-locked titanium−sapphire laser with wavelengths of 770 and 800 nm for SapRC2 and CRC2, respectively. The laser power was tuned to produce sufficient fluorescent signal from the donors. The red cameleons were distributed evenly in the cytosol, with no signs of aggregation. Transient rises in $[Ca^{2+}]_c$ were observed when the cells were stimulated with histamine (10 μM). However, the emission ratios of YRC2 (Figure 8A) and CRC2 (Figure 8B) gradually fell to levels that were below the prestimuli baselines. By contrast, the emission ratio of SapRC2 rose and fell reversibly (Figure 8C). Thus, meaningful R_{max} and R_{min} values were obtained in the experiments using SapRC2.

Red Cameleons Expressed in Primary Neurons. YRC2 and SapRC2 were expressed in dissociated hippocampal neurons, in which not only elevation in $[Ca^{2+}]_c$ but also decrease in intracellular pH occurs by glutamate and/or depolarization stimuli. Imaging was performed using a conventional microscope. Figure 9A shows the spontaneous oscillation in $[Ca^{2+}]_c$ observed in a neuron expressing YRC2. The neuron was connected with several other neurons, and oscillatory changes in $[Ca^{2+}]_c$ occurred synchronously in all the neurons. The oscillations were augmented when the neurons were stimulated with 1 μM glutamate and suppressed by the application of 1 μM TTX. A slight drop in the baseline of donor signals (the fluorescence of EYFP-V68L/Q69K) was observed after glutamate stimulation (Figure 9B). Transient changes in $[Ca^{2+}]_c$ induced by depolarization were compared in YRC2-expressing and SapRC2-expressing neurons. The application of 20 mM KCl was shown to decrease the intracellular pH by 0.2−0.4. In addition to the Ca^{2+} response, the fluorescence of EYFP-V68L/Q69K (the donor of YRC2) was suppressed for over 300 s (Figure 10B), whereas no long-term effects on the fluorescence of DsRed were observed. Therefore, the decay in the $[Ca^{2+}]_c$ transient was judged to be very slow (Figure 10A). In contrast, the fluorescent signals of Sapphire and DsRed changed reciprocally (Figure 10D), and the emission ratio of SapRC2 quickly returned to the basal level (Figure 10C).

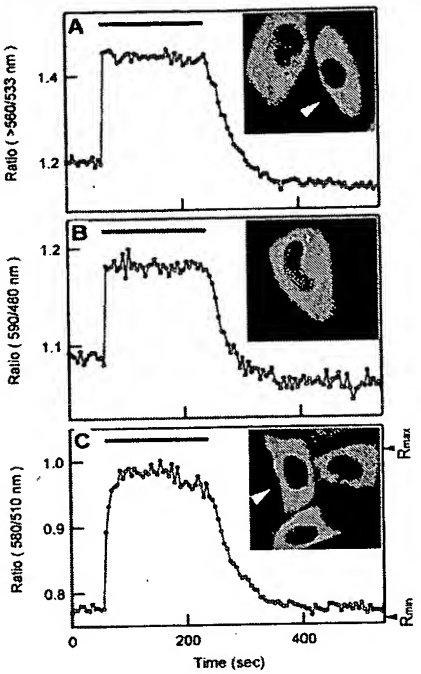

FIGURE 8: Histamine-induced $[Ca^{2+}]_c$ transients in HeLa cells expressing YRC2 (A), CRC2 (B), and SapRC2 (C). In (A) and (C), traces were obtained from cells indicated with white arrow heads. Insets show fluorescence images acquired through the donor channels described in Table 1. Perfusate was changed to buffer containing 10 μM histamine during the time indicated with bars. R_{max} and R_{min} values are indicated on the right (C).

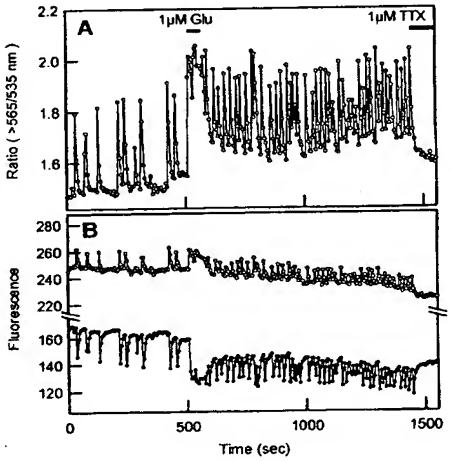

FIGURE 9: Oscillation in $[Ca^{2+}]_c$ observed in a hippocampal neuron-expressing YRC2. (A) Ratio of >565-nm to 535-nm emissions. (B) >565-nm (open circles) and 535-nm (closed circles) emissions. Perfusate was changed to buffer containing 1 μM glutamate (Glu) or 1 μM tetrodotoxin (TTX) during the time indicated in (A).

DISCUSSION

The fluorophores for multi-labels and FRET should have sharp excitation and emission spectra, allowing cross-excitation or cross-detection to be minimized. However, DsRed shows broad and complex spectra. The fluorophores

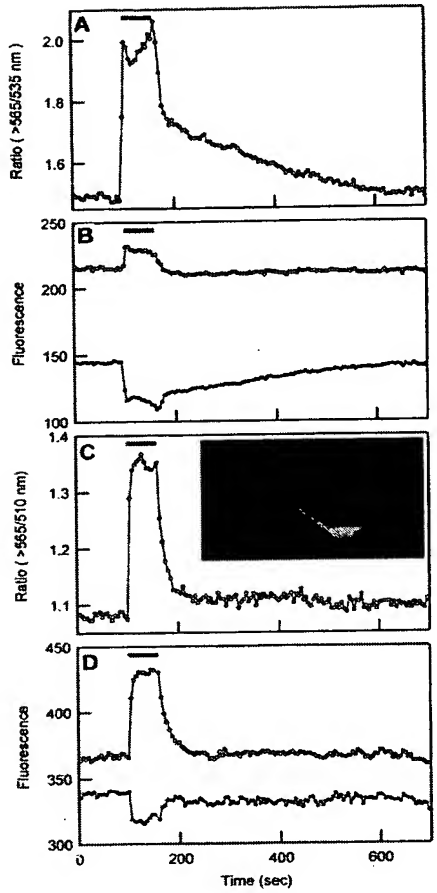

FIGURE 10: Depolarization-induced $[Ca^{2+}]_c$ transients in hippocampal neurons expressing YRC2 (A and B) and SapRC2 (C and D). The inset in (C) shows a fluorescence image of the neuron expressing SapRC2 acquired through the donor channel described in Table 2. (A) Ratio of >565-nm to 535-nm emissions. (C) Ratio of >565-nm to 510-nm emissions. (B and D) Individual emissions of acceptor (open circles) and donor (closed circles). Perfusate was changed to the buffer containing 20 mM KCl during the time indicated with bars.

functioning as fusion tags are required not to form a multimer complex; otherwise proteins with the tags might show altered functions or distributions. However, DsRed forms a stable homotetramer complex. In the present study, we investigated the spectral and structural properties of DsRed, and examined how these properties affected the usefulness of DsRed for fluorescence imaging.

Our spectral analyses revealed DsRed to have two fluorescent components: one component emitting at 583 nm, and the other emitting at 500 nm. Although the 583-nm peak is always predominant, the recombinant DsRed produced in *E. coli* at RT had a significant amount of the subcomponent emitting at 500 nm. We found that incubation at 37 °C caused a transition from green (the subcomponent) to red (the main component), thereby increasing the amplitude of the 583-nm peak, at the expense of the 500-nm peak. The temporal profile of the transition suggests that there are two states: one favors the main component, and the other the subcom-

ponent. We did not detect the shift from red to green when we incubated $DsRed_{37,75,s}$ at various temperatures and pHs. Since the transition was always unidirectional, we assume that it reflects maturation of DsRed. The more rapid maturation of DsRed at 37 °C than at RT contrasts with the better folding of *Aequorea* GFP at lower temperatures. Such a difference could be explained by the temperature of the water in which the organisms live; *Aequorea victoria* in Puget Sound vs *Discosoma* in the Indo-Pacific ocean (*3*, *15*). Although the two fluorescent components are complex, and barely separable, a comparison of the emission spectra excited at 277 nm between $DsRed_{37,75,s}$ and $DsRed_{RT,24,p}$ does give some information. The emission peak at 330 nm was less significant in the spectrum of $DsRed_{37,75,s}$ than in that of $DsRed_{RT,24,p}$. The 277-nm light probably excites three tryptophans in DsRed (W58, W93, and W143). Since there is a spectral overlap between the emission of tryptophan and the absorption spectrum of the main component around 330 nm, the excited-state energy of the tryptophans should be used to produce the main component.

In the wild-type *Aequorea* GFP, there coexist neutral and anion chromophores, which give two absorption peaks at 395 and 475 nm. A subset of mutations has simplified the spectra to single absorption peaks at either 395 or 475 nm (*2*). We were interested in obtaining mutants of DsRed that would mature quickly. Such mutants should be purely red, and desirable for almost all cell−biological applications. However, every randomly introduced mutation slowed the maturation process. One representative mutant was DsRed-mu43 (Y120H/K168R), in which the subcomponent always predominated.

To what extent is the presence of the subfluorescent component of concern in general cell biological studies? The subcomponent was not detected in HeLa cells. Thus, DsRed proteins expressed in mammalian cells are likely to mature very rapidly, so long as the cells are kept at 37 °C. However, the rate of DsRed maturation might be regulated by factors other than incubation temperature, including the effect of fusion to other proteins. It should be noted that even without the subcomponent, the excitation spectrum of the mature DsRed (the main component) is broad. Therefore, the current DsRed suffers from cross-excitation when shorter wavelength GFPs are illuminated in multilabel and FRET experiments.

The native DsRed is composed of four polypeptide chains associated through noncovalent bonds. It is interesting to study the inter-relationships between chromophore formation and chain folding or chain association. Size-exclusion chromatography and multiangle light scattering analysis detected only one molecular species, which was the fluorescent tetrameric complex of DsRed. No intermediate species such as the monomer and dimer DsRed were observed at the protein level. These findings suggest that the synthesized DsRed protein is tetramerized very quickly. In addition, since sensitive fluorescence detection did not recognize any intermediates, DsRed probably becomes fluorescent after forming the tetrameric complex. Oligomeric association is possibly necessary for chromophore formation and maturation (the conversion from green to red). Furthermore, we did not succeed in partial or total dissociation of the DsRed complex while maintaining the fluorescence, using moderate concentrations of denaturants (8 M urea and 6 M guanidinium chloride), a detergent (1% SDS), reductants (0.1 M DTT and 0.1 M β-mercaptoethanol), and extremes of pH (pH 3). It was therefore suggested that the tetrameric complex is required to maintain fluorescence.

Generally a globular protein larger than 60 kDa is hardly able to enter the nucleus. Although DsRed forms a tetrameric complex of 115 kDa, the red fluorescence was distributed homogeneously through both the cytosol and nucleus of HeLa cell. Because the tetrameric complex species was exclusively predominant in the cell extract, it is less likely that there was an equilibrium between the tetramer and dimer or monomer, and that such small molecules passed throughout the nuclear pores. An alternative explanation is that the DsRed tetramer is not globular, but taking certain shape so that it can pass freely through the cylindrical channel about 9 nm in diameter. The peculiar structure of DsRed tetramer was suggested from its hydrodynamic behavior; size-exclusion chromatography estimated the smaller molecular mass (75.6 kDa).

In this study, we tried a differential detection of CaM-fused CFP and DsRed expressed in single cells. It was shown that CFP was selectively excited over YFP by a femtosecond-pulsed Ti:sapphire laser in the excitation wavelength range of 770−810 nm (*16*). How can we image the fluorescence of DsRed with two-photon excitation microscopy? Although it is difficult to make quantitative predictions about the behavior of two-photon absorption from the one-photon spectrum, assuming that the structure of the DsRed chromophore was not symmetrical, we expected that DsRed could be excited at the wavelength of twice the one-photon absorption maximum (558 nm). We used an Nd:YLF laser (1047 nm in 170 fs pulses at a repetition rate of 120 MHz). Two laser beams from a Ti:sapphire laser (800 nm in 80−100 fs pulses) and the Nd:YLF laser were alternately used to excite ECFP and DsRed, respectively. Then we observed that DsRed−CaM and ECFP−CaM were differently distributed in single HeLa cells. The cytoplasmic aggregation of the DsRed−CaM, however, does not necessarily mean that DsRed is inappropriate as a tag onto CaM. Making soluble fusion proteins of CaM and DsRed by switching the order of the two protein domains with various linkers is now underway.

We noticed significant bleaching of DsRed while we imaged cells using laser scanning confocal microscopy, while when HeLa cells expressing DsRed were illuminated with strong light from a xenon lamp through a 550DF30 filter (0.74 W/cm^2), the red fluorescence was not significantly bleached within 1 h (H.M., A.S., and A.M., unpublished results). Therefore, we assume that DsRed is relatively more sensitive to brief but extremely intense bursts of excitation light than to continuous-illumination light, although bleaching of fluorophore is a complex phenomenon and is related to many factors, such as light intensity, illumination time, oxygen concentrations, etc.

When DsRed is used as an acceptor for FRET, the following two characteristics of DsRed which we found in the present study should be taken into consideration.

(1) DsRed exhibits a broad excitation spectrum, even after maturation. In addition to an excitation maximum at 558 nm, several peaks and shoulders in the shorter wavelength region are present. Therefore, DsRed is not an ideal acceptor for FRET; cross-excitation of DsRed may affect the signal obtained through the FRET channel.

(2) DsRed is pH-resistant. In this respect, a pH-resistant FRET can be obtained if the donor GFP has a pH-insensitive quantum yield (*17*).

The combination of YFP and DsRed suffers from a cross-excitation of acceptors. Both the 488-nm laser beam of argon and illumination with light from a xenon lamp through a 480DF10 filter directly excited a large amount of DsRed. Therefore, the relative sensitivity to pH and light of YFP and DsRed affects the ratio value of the two emission signals. Figure 8A shows one example, in which the 488-nm laser bleached DsRed more than YFP (EYFP-V68L/Q69K) of YRC2; in another experiment using HeLa cells illuminated with the light through a 480DF10 filter, EYFP-V68L/Q69K was more bleached than DsRed of YRC2 (results not shown), suggesting again the vulnerability of DsRed to laser light. On the other hand, only EYFP-V68L/Q69K was quenched by acidification in primary neurons expressing YRC2 (Figures 9A,B and 10A,B). In all cases, the emission ratio curves were disturbed. Without such cross-excitation, the bleaching and pH sensitivity of YFP would not be a concern because the decrease in the number of YFP molecules or pH-dependent changes in the absorbance of YFP would not affect the FRET efficiency (*17*).

Cross-excitation of DsRed was also seen when cells were illuminated through a 440DF20 filter and with an 800-nm beam from a pulsed laser, both of which were used with the intention of excitating CFP selectively. While ECFP was relatively photostable against the 800-nm beam from a Ti:sapphire laser, DsRed was noticeably bleached; therefore, the ratio value (590/480 nm) gradually fell (Figure 8B). Also, CFP is not an ideal donor because of its pH-sensitive quantum yield (*17*).

Sapphire is thought to be a good donor because it is resistant to pH (pK_a = 5.5) (*17*) and light, and exhibits a large Stoke's shift (*8*). It should be noted that DsRed is not excited by light around 400 nm, which is the most effective wavelength for exciting Sapphire. Thus, the pairing of Sapphire−DsRed would not suffer from the above-mentioned cross-excitation. Two-photon excitation using a 770-nm-pulsed laser (Figure 8C) and light through a 400DF15 filter (Figure 10C,D) produced stable baselines. Although substitution of EYFP-V68L/Q69K for EYFP reduced the pH-sensitivity of the most popular cameleons, yellow cameleons to some extent (*7*), more pH-resistant cameleons have been desired. For instance, neuronal activity gives rise to significant acidification in neuronal cells during depolarization and glutamate stimulation. Since both Sapphire and DsRed are indifferent to pH changes, the red cameleon containing the two proteins enabled the quantitative measurement of $[Ca^{2+}]_c$ in hippocampal neurons (Figure 10C,D).

A general advantage of using *Aequorea* GFP and DsRed for FRET would be that there is less interaction between the donor and the acceptor than between two *Aequorea* GFP variants. However, our MALS analysis revealed a high molecular mass (approximately 300 kDa) for the red cameleons, indicating their homotetrameric formation. Although the present study demonstrates that they can work as Ca^{2+} indicators despite the oligomerization, the use of the current DsRed as a FRET acceptor would not be suitable for monitoring intermolecular protein−protein interactions in single living cells.

ADDED IN PROOF

Three reports published following the submission of paper have characterized the biochemistry (*18*) and photophysics (*19*) of DsRed, and determined the structure of its chromophore (*20*).

ACKNOWLEDGMENT

We thank Dr. M. Nakamura and Dr. R. Ohno for acquiring MALS data, and Dr. T. Arakawa and Dr. M. Ikura for fruitful discussions.

REFERENCES

1. Hastings, J. W., and Morin, J. G. (1998) in *Green Fluorescent Protein* (Chalfie, M., and Kain, S., Eds.) pp 17−41, Wiley-Liss, Inc., New York.
2. Tsien, R. Y. (1998) *Annu. Rev. Biochem. 67*, 509−544.
3. Matz, M. V., Fradkov, A. F., Labas, Y. A., Savitsky, A. P., Zaraisky, A. G., Markelov, M. L., and Lukyanov, S. A. (1999) *Nat. Biotechnol. 17*, 969−973.
4. Ward, W. W. (1998) in *Green Fluorescent Protein* (Chalfie, M., and Kain, S., Eds.) pp 45−75, Wiley-Liss, Inc., New York.
5. Ward, W. W., Prentice, H. J., Roth, A. F., Cody, C. W., and Reeves, S. C. (1982) *Photochem. Photobiol. 35*, 803−808.
6. Miyawaki, A., Llopis, J., Heim, R., McCaffery, J. M., Adams, J. A., Ikura, M., and Tsien, R. Y. (1997) *Nature 388*, 882−887.
7. Miyawaki, A., Griesbeck, O., Heim, R., and Tsien, R. Y. (1999) *Proc. Natl. Acad. Sci. U.S.A. 96*, 2135−2140.
8. Heim, R. (1999) *Methods Enzymol. 302*, 408−423.
9. Cadwell, R. C., and Joyce, G. F. (1992) *PCR Methods Appl. 2*, 28−33.
10. Heim, R., and Tsien, R. Y. (1996) *Curr. Biol. 6*, 178−182.
11. Wyatt, P. J. (1993) *Anal. Chim. Acta 272*, 1−40.
12. Kossel, A. H., Williams, C. V., Schweizer, M., and Kater, S. B. (1997) *J. Neurosci. 17*, 6314−6324.
13. Kakinuma, Y., Hama, H., Sugiyama, F., Goto, K., Murakami, K., and Fukamizu, A. (1997) *Neurosci. Lett. 232*, 167−170.
14. Rouget, P., Le Bert, M., Borde, I., and Evrard C. (1992) in *Neuronal Cell Lines* (Wood, J. N., Ed.) pp 27−54, IRL Press, Oxford, U.K.
15. Tsien, R. Y., and Prasher, D. C. (1998) in *Green Fluorescent Protein* (Chalfie, M., and Kain, S., Eds.) pp 97−118, Wiley-Liss, Inc., New York.
16. Fan, G. Y., Fujisaki, H., Miyawaki, A., Tsay, R.-K., Tsien, R. Y., and Ellisman, M. H. (1999) *Biophys. J. 76*, 2412−2420.
17. Miyawaki, A., and Tsien, R. Y. (2000) *Methods Enzymol. 327*, 472−500.
18. Baird, G. S., Zacharias, D. A., and Tsien, R. Y. (2000) *Proc. Natl. Acad. Sci. U.S.A. 97*, 11984−11989.
19. Heikal, A. A., Hess, S. T., Baird, G. S., Tsien, R. Y., and Webb, W. W. (2000) *Proc. Natl. Acad. Sci. U.S.A. 97*, 11996−12001.
20. Gross, L. A., Baird, G. S., Hoffman, R. C., Baldridge, K. K., and Tsien, R. Y. (2000) *Proc. Natl. Acad. Sci. U.S.A. 97*, 11990−11995.

BI002263B

Biochem. J. (2004) 381, 307–312 (Printed in Great Britain)

Cyan-emitting and orange-emitting fluorescent proteins as a donor/acceptor pair for fluorescence resonance energy transfer

Satoshi KARASAWA*†‡, Toshio ARAKI*†‡, Takeharu NAGAI*§, Hideaki MIZUNO* and Atsushi MIYAWAKI*[1]

*Laboratory for Cell Function and Dynamics, Advanced Technology Development Group, Brain Science Institute, RIKEN, 2-1 Hirosawa, Wako-city, Saitama, 351-0198, Japan, †Amalgaam Co. Ltd, 2-9-3 Itabashi, Itabashi-ku, Tokyo, 173-0004, Japan, ‡Medical & Biological Laboratories Co. Ltd, 3-5-10 Marunouchi, Naka-ku, Nagoya-city, 460-0002, Japan, and §Structure and Function of Biomolecules, PRESTO, JST, 4-1-8 Hon-cho, Kawaguchi, Saitama, 332-0012, Japan

GFP (green fluorescent protein)-based FRET (fluorescence resonance energy transfer) technology has facilitated the exploration of the spatio-temporal patterns of cellular signalling. While most studies have used cyan- and yellow-emitting FPs (fluorescent proteins) as FRET donors and acceptors respectively, this pair of proteins suffers from problems of pH-sensitivity and bleeding between channels. In the present paper, we demonstrate the use of an alternative additional donor/acceptor pair. We have cloned two genes encoding FPs from stony corals. We isolated a cyan-emitting FP from *Acropara* sp., whose tentacles exhibit cyan coloration. Similar to GFP from *Renilla reniformis*, the cyan FP forms a tight dimeric complex. We also discovered an orange-emitting FP from *Fungia concinna*. As the orange FP exists in a complex oligomeric structure, we converted this protein into a monomeric form through the introduction of three amino acid substitutions, recently reported to be effective for converting DsRed into a monomer (Clontech). We used the cyan FP and monomeric orange FP as a donor/acceptor pair to monitor the activity of caspase 3 during apoptosis. Due to the close spectral overlap of the donor emission and acceptor absorption (a large Förster distance), substantial pH-resistance of the donor fluorescence quantum yield and the acceptor absorbance, as well as good separation of the donor and acceptor signals, the new pair can be used for more effective quantitative FRET imaging.

Key words: donor/acceptor pair, fluorescence resonance energy transfer (FRET), green fluorescent protein (GFP), green fluorescent protein (GFP)-like protein.

INTRODUCTION

While spectral variant proteins with blue, cyan and yellow-green emissions have been generated from the bioluminescent jellyfish, *Aequorea victoria* [1], the discovery of GFP (green fluorescent protein)-like proteins from Anthozoa has significantly expanded the range of colours available for biotechnological applications. In 1999, Matz et al. [2] cloned six anthozoan naturally FPs (fluorescent proteins), all of which had 26–30 % identity with *Aequorea* GFP. One of the novel FPs cloned from a red *Discosoma* species, drFP583, commercially known as DsRed, was demonstrated to show red-shifted excitation and emission spectra. The family of 'GFP-like proteins' continues to expand further [3,4]. To date, over 30 significantly different family members have been reported. In addition to sharing a modest degree of sequence identity, all GFP-like proteins probably share the same general β-can fold and possess intrinsic chromophores [3].

In the present paper, we present the molecular cloning and characterization of two FPs from stony coral animals, a CFP (cyan FP) derived from *Acropara* sp. and an orange FP from *Fungia concinna*. We utilized these two FPs as a novel donor/acceptor pair for FRET (fluorescence resonance energy transfer) measurements detecting caspase 3 activity during an apoptotic process. The performance of this donor/acceptor pair is highly effective, possibly proving to be as useful an experimental system as the common CFP/YFP (yellow FP) pair.

EXPERIMENTAL

cDNA cloning and gene construction

Samples of the *Acropara* and *Fungia* stony corals were acquired from the ocean near the Okinawa islands by Dr K. Iwao (Akajima Marine Science Laboratory, Okinawa, Japan). Total RNA was isolated from the corals by guanidine thiocyanate extraction [5]. Synthesis, amplification using degenerate primers, and generation of full-length cDNA were performed as previously described [2] using the following degenerate primers: 5′-GAAGGRT-GYGTCAAYGGRCAY-3′ and 5′-ACVGGDCCATYDGVAAG-AAARTT-3′. The cDNA encoding the protein-coding region was amplified using primers containing 5′ *Bam*HI and 3′ *Eco*RI sites. The digested product was then cloned in-frame into the *Bam*HI/*Eco*RI sites of pRSETB for bacterial expression. The 5′ end of the gene was modified by PCR to contain a Kozak consensus sequence (CCACCATG) after the *Bam*HI site to promote efficient transcription. The *Bam*HI/*Eco*RI fragment was then subcloned into the mammalian expression vector, pcDNA3 (Invitrogen).

Mutagenesis

Site-directed and semi-random mutations were introduced as described [6]. For semi-random mutants, multiple degenerative

Abbreviations used: CCD, charge-coupled device; CFP, cyan fluorescent protein; ECFP, enhanced CFP; FP, fluorescent protein; FRET, fluorescence resonance energy transfer; GFP, green fluorescent protein; KO, Kusabira-Orange; mKO, monomeric KO; MiCy, Midori-ishi cyan; mRFP1, monomeric red fluorescent protein; YFP, yellow fluorescent protein.

[1] To whom correspondence should be addressed (e-mail matsushi@brain.riken.go.jp).

The nucleotide sequences reported have been deposited in the DDBJ, EMBL, GenBank® and GSDB Nucleotide Sequence Databases under accession numbers AB128819 (KO), AB128820 (KO with an artificial Met-Ser-Val-Ile-Lys-Pro-Glu amino acid sequence at the N-terminus), AB128821 (monomeric KO) and AB128822 (MiCy).

primers were used to mutate amino acid residues at multiple sites simultaneously.

Protein expression, *in vitro* spectroscopy and pH titrations

Proteins were expressed in *Escherichia coli*, purified, and characterized spectroscopically as described previously [7]. Fluorescence quantum yields were determined using fluorescein as a standard (0.91). For calculation of molar absorption coefficients, protein concentrations were measured using a Bradford assay kit (Bio-Rad) with BSA as the standard. pH titrations were performed as described [7].

Analytical ultracentrifugation

Sedimentation equilibrium experiments were performed using a Beckman An60Ti rotor on a Beckman XL-I analytical ultracentrifuge at 25 °C. Absorbance was measured at the maximum wavelength as a function of radius at 25 000 rev./min. Using this system, the tetramerization of DsRed [8] was verified.

Fluorescence imaging

HeLa cells were grown on 35-mm glass-bottom dishes in Dulbecco's modified Eagle's medium containing 10 % (v/v) foetal bovine serum. At 2–4 days after transfection with Polyfect (Qiagen), cells in Hanks balanced salt solution buffer (Gibco) were treated with 500 ng/ml anti-Fas antibody: (CH-11; Medical & Biological Laboratories Co. Ltd), then subjected to imaging. FRET images were acquired on the Aquacosmos/Ashura system (Hamamatsu Photonics) using an IX-71 inverted microscope equipped with a Uapo 340 40 × 1.35 NA oil-immersion objective (Olympus), a 440AF21 excitation filter, a 455DRLP dichroic mirror, a 480 ALP emission filter and a three CCD (charge-coupled device) colour camera (C7780-22; Hamamatsu Photonics). Image acquisition and analysis were performed using Aquacosmos 2.5 software (Hamamatsu Photonics).

RESULTS AND DISCUSSION

Two fluorescent coral animals were collected in the Okinawa islands. *Acropara* sp. shows cyan coloration in the tips of its tentacle. *Fungia concinna* emits an orange fluorescence from its whole body. Degenerate primers served to amplify cDNAs from the samples. The primers represented variations of several regions whose amino acid sequences are conserved among GFP-like fluorescent proteins from Anthozoa species. The missing 5′ and 3′ ends of the cDNA fragments were amplified using RACE (rapid amplification of cDNA ends). cDNA clones #301 and #11 were obtained from *Acropara* sp. and *F. concinna* respectively.

A CFP, MiCy

Based on amino acid alignment (Figure 1), clone #301 appeared to encode the full-length protein. Transformation of the isolated cDNA into *E. coli* produced bright cyan colonies. The addition of a His_6 tag at the N-terminus of the protein allowed purification using metal-affinity chromatography. As the protein, derived from the *Acropara* organism whose Japanese name is Midori-ishi, emitted cyan fluorescence, we named this novel FP MiCy. The closest orthologue is amFP486, a CFP cloned from *Anemonia majano* [2], which shares 48.2 % identity. Similar to amFP486, MiCy possesses a tyrosine residue at the second amino acid of the chromophore-forming tripeptide, while ECFP (enhanced CFP) has a tryptophan residue at this position. The absorption spectrum

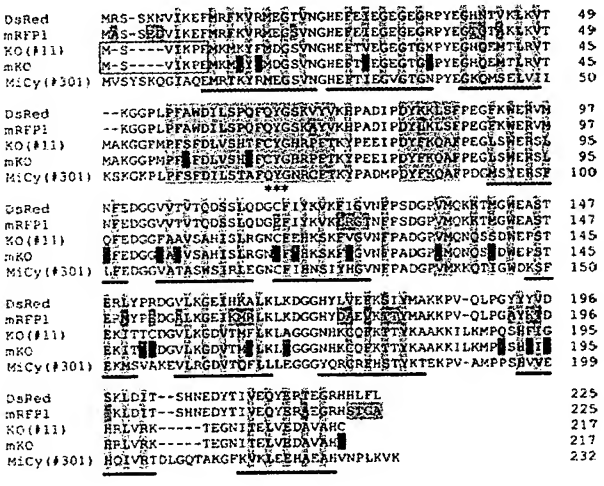

Figure 1 Amino acid sequence (single-letter code) alignment of DsRed, mRFP1, KO, mKO and MiCy

In the sequence of MiCy, the β-sheet-forming regions are underlined. Residues whose side chains form the interior of the β-can [20] are shaded in grey. In the mRFP1 sequence, the substituted amino acids are shaded in yellow. In the sequence of mKO, the substituted amino acids that disrupt dimeric structure, increase folding efficiency and inhibit aggregation are shaded in blue, red and green respectively. In the sequences of both KO and mKO, the artificial regions are boxed in red. The residues responsible for chromophore synthesis are indicated by an asterisk.

of MiCy at pH 7.4 displayed two peaks, one at 472 nm ($\varepsilon =$ 27 250 $M^{-1} \cdot cm^{-1}$) and one at 380 nm ($\varepsilon = 15\,000\ M^{-1} \cdot cm^{-1}$) (Figure 2A). With decreasing pH, the amplitude of the 472-nm peak decreased, while that of the 380-nm peak increased concomitantly, exhibiting an isosbestic point at 413 nm (results not shown). This pH-dependency indicates that the 380- and 472-nm peaks correspond to the neutral and ionized states of the phenolic hydroxy group of the chromophore respectively [1]. The protein had an apparent pK_a of 6.6 (Figure 2D).

Excitation and emission spectra of MiCy are displayed in Figure 3(A). While the neutral form of the protein was non-fluorescent, the ionized form was highly fluorescent; the fluorescence quantum yield (Φ) was determined to be 0.90. The fluorescence spectra displayed the same pH dependency as the absorption spectrum, indicating that the Φ of MiCy was pH-resistant. Due to the high value and pH-resistance of the Φ, MiCy would probably be a more efficient and reliable donor for FRET than ECFP. In addition, fluorescence lifetime measurement revealed that MiCy fluorescence displayed as a single exponential decay with a time constant of 3.4 ns (Table 1). In contrast, ECFP exhibits a bi-exponential decay with 1.6 ns and 3.9 ns time constants. The simplicity of MiCy excited-state fluorescence decay makes it an ideal donor for fluorescence lifetime imaging experiments.

We determined the absolute molecular mass of MiCy to be 59.7 kDa by analytical equilibrium ultracentrifugation analysis (Figure 4A). This value was twice as large as larger than the value (29.9 kDa) deduced from the primary structure of the protein, suggesting that MiCy forms a homodimeric complex similar to GFP from the bioluminescent sea pansy, *Renilla reniformis* [9]. Since all of the non-bioluminescent Anthozoan GFP-like proteins characterized so far form obligate tetramers [3], the dimer formation of MiCy may indicate structural divergence of the protein family.

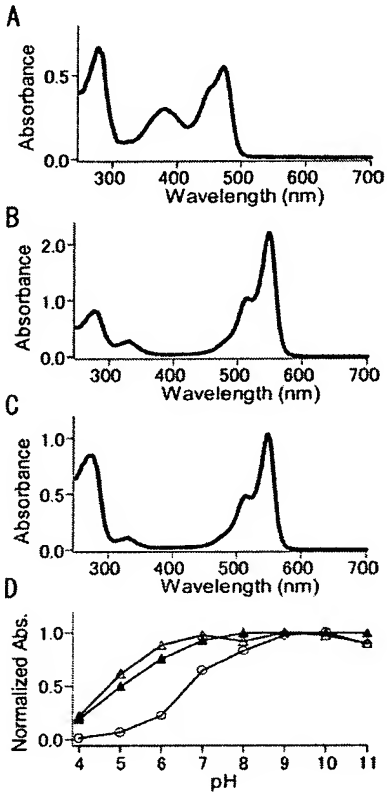

Figure 2 Light-absorption properties of the new fluorescent proteins

Absorption spectra of MiCy (**A**), KO (**B**) and mKO (**C**), and the pH-dependence of the absorption (Abs.) peak at the maximum (**D**).

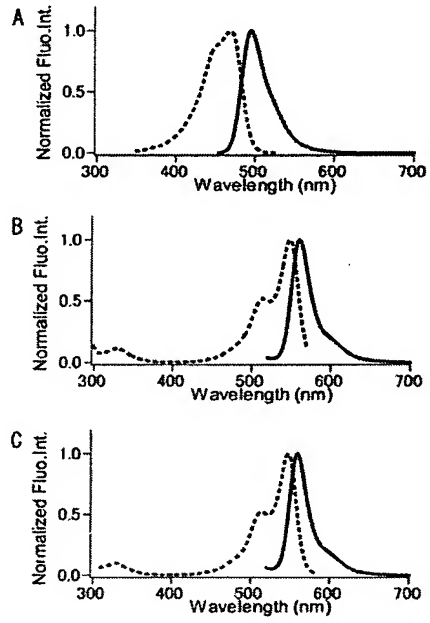

Figure 3 Normalized excitation (broken line) and emission (solid line) spectra of MiCy (A), KO (B) and mKO (C)

Fluo.Int., fluorescence intensity.

An orange fluorescent protein, KO (Kusabira-Orange)

The cDNA clone from *F. concinna* (#11) demonstrates 46.7% identity with amFP486. Upon transformation into *E. coli*, however, no fluorescent colonies were formed. Sequence alignment revealed that, in reference to other FPs, the encoded protein lacked approximately ten amino acids at the N-terminus. We therefore attached an artificial amino acid sequence, Met-Ser-Val-Ile-Lys-Pro-Glu, to the N-terminus (Figure 1). The resulting protein produced bright orange fluorescent bacterial colonies. As *F. concinna* is known in Japanese as Kusabira-Ishi, we named the protein Kusabira-Orange (KO).

We analysed the spectral properties of recombinant KO prepared from bacteria. At pH 7.4, KO displayed a major absorption wavelength maximum at 548 nm ($\varepsilon = 109750\ M^{-1} \cdot cm^{-1}$) with a slight shoulder at 515 nm (Figure 2B). The large value of the molar absorption coefficient suggested the efficient maturation of the chromophore. A green-fluorescent intermediate appeared transiently in the course of chromophore maturation of KO, as seen for DsRed (results not shown). At significantly low pHs, an emission peak was also detected at approx. 423 nm. The relative intensities of these two absorption peaks changed with pH, indicating that the 423- and 548-nm peaks correspond to the neutral and ionized states of the phenolic hydroxy group of the chromophore respectively. The absorption spectrum of KO was pH-insensitive; the apparent pKa was determined to be below 5.0 (Figure 2D). Excitation and emission spectra of KO are shown in Figure 3(B). Following excitation at 500 nm, the protein emitted a bright orange fluorescence, peaking at 561 nm. The fluorescence intensity decreased slightly with increasingly acidic pH, exhibiting a similar apparent pK_a (< 5.0) as seen for the absorption spectrum. Thus the fluorescence quantum yield ($\Phi = 0.45$) is not pH-sensitive. We subjected the KO protein to analytical equilibrium ultracentrifugation analysis to calculate the absolute molecular mass of 77.0 kDa. This value was 2.75 times larger than that (28.0 kDa) deduced from the primary structure

Table 1 Biochemical and spectral properties of ECFP, MiCy, KO and mKO

Protein	Excitation/emission maxima (nm)	Molar absorption coefficient ($M^{-1} \cdot cm^{-1}$)	Fluorescence quantum yield	pH-sensitivity (pK_a)	Fluorescence lifetime (ns)	Number of amino acids
ECFP	435/478	28750 (435 nm)	0.40	5.5 (Φ)	1.60, 3.90	238
MiCy	472/495	27250 (472 nm)	0.90	6.6 (ε)	3.4	232
KO	548/561	109750 (548 nm)	0.45	< 5.0 (ε)	4.2	217
mKO	548/559	51600 (548 nm)	0.60	5.0 (ε)	4.1	217

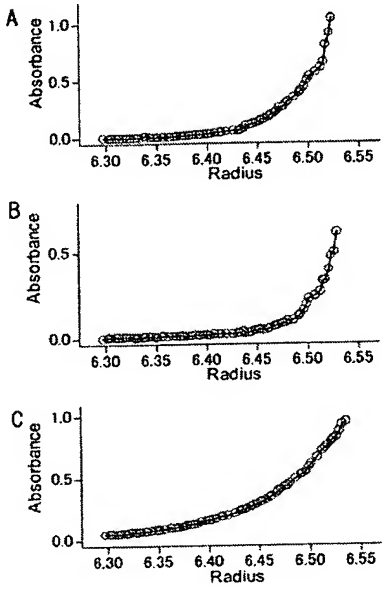

Figure 4 The equilibrium radial absorbance profiles at 25 000 rev./min by analytical ultracentrifugation analysis for MiCy (59.7 kDa) (A), KO (77.0 kDa) (B), and mKO (28.1 kDa) (C)

of the protein, suggesting that KO may exist in a heterogeneous oligomeric state, including dimers and tetramers.

Due to the development of new techniques allowing efficient discrimination of distinct fluorophores with overlapping emission spectra, such as the linear unmixing method [10], any small shift in the emission spectrum of novel FPs from established proteins would make the protein useful. Besides, there is a gap between green and red or between yellow and orange-red in the emission spectra of *Aequorea* GFP variants and GFP-like proteins from Anthozoa. Thus a true orange FP, such as KO, may greatly expand the repertoire of fluorescent dyes available for multicolour imaging.

Construction of a monomeric version of KO, mKO

A monomeric version of DsRed, called mRFP1, was previously generated by alteration of 33 amino acids [11]. KO has endogenous amino acid residues corresponding to six of the substitutions: $Thr^{21} \rightarrow$ Ser, $Asn^{42} \rightarrow$ Gln, $Lys^{163} \rightarrow$ Met, $Ser^{179} \rightarrow$ Thr, $Ile^{180} \rightarrow$ Thr and $Thr^{217} \rightarrow$ Ala (numbering is based on DsRed). Assuming that the KO oligomer exhibits a similar structure to the DsRed tetramer, we introduced three mutations ($Phe^{102} \rightarrow$ Ser, $Ala^{104} \rightarrow$ Ser and $Val^{123} \rightarrow$ Thr) into the AB interface and four mutations ($Cys^{151} \rightarrow$ Ser, $Phe^{162} \rightarrow$ Tyr, $Phe^{193} \rightarrow$ Tyr and $Gly^{195} \rightarrow$ Ser) into the AC interface of KO. We then performed additional mutagenesis to obtain a brighter KO molecule. Twelve mutations ($Lys^{11} \rightarrow$ Arg, $Val^{25} \rightarrow$ Ile, $Lys^{32} \rightarrow$ Arg, $Ser^{55} \rightarrow$ Ala, $Thr^{62} \rightarrow$ Val, $Gln^{96} \rightarrow$ Glu, $Glu^{117} \rightarrow$ Tyr, $Val^{133} \rightarrow$ Ile, $Ser^{139} \rightarrow$ Val, $Thr^{150} \rightarrow$ Ala, $Ala^{166} \rightarrow$ Glu and $Gln^{190} \rightarrow$ Gly) and three mutations ($Phe^{13} \rightarrow$ Tyr, $Cys^{115} \rightarrow$ Thr and $Cys^{217} \rightarrow$ Ser) were introduced to increase the folding efficiency and the solubility of the mutants respectively (Figure 1). The resulting protein retained the original bright orange fluorescence. The absolute molecular mass of 28.1 kDa (Figure 4C), determined by analytical equilibrium ultracentrifugation, is almost identical with the predicted size (28.0 kDa). This molecule was named mKO.

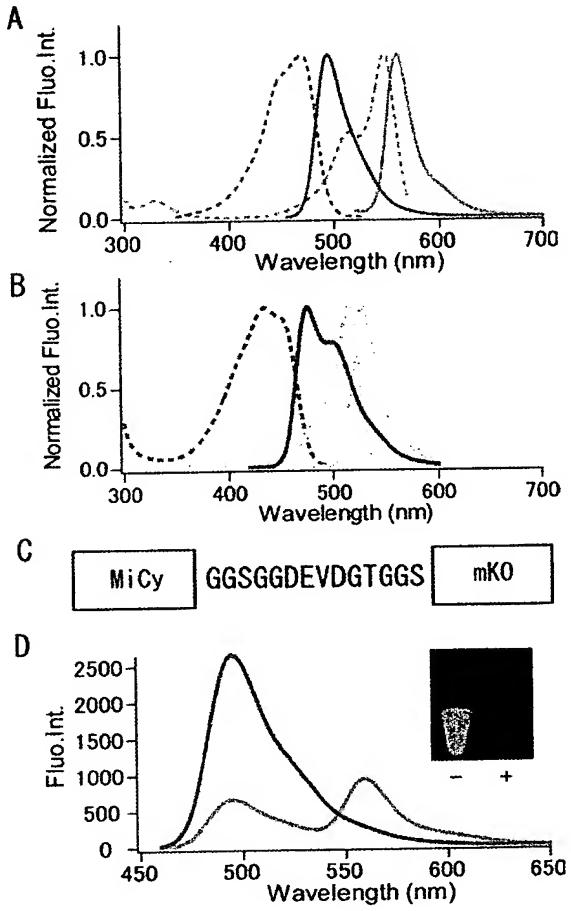

Figure 5 FRET between MiCy and mKO

(**A**) Normalized excitation (broken line) and emission (solid line) spectra of MiCy and mKO. (**B**) Normalized excitation (broken line) and emission (solid line) spectra of CFP and YFP. (**C**) Primary structure of the caspase-3-sensor protein. (**D**) Emission spectra of the caspase-3-sensor with excitation at 440 nm before (light grey) and after (dark grey) incubation with caspase 3. Inset, overt appearance of the sample tubes. Fluo.Int., fluorescence intensity.

mKO exhibited similar fluorescence properties to KO (Figures 2C and 3C), but demonstrated a small decrease in light-absorbing ability ($\varepsilon = 51\,600\ M^{-1} \cdot cm^{-1}$ at 548 nm) and a slight decrease in pH-resistance (apparent $pK_a = 5.0$) (Figure 2D). mKO also exhibits a higher fluorescence quantum yield than KO (0.60 compared with 0.45). Similar improvements in the fluorescence quantum yield were observed following oligomer into monomer conversion of a subset of Anthozoa fluorescent proteins, such as AG (Azami-Green) [12], although the production of mRFP1 was accompanied by decreased quantum yield [11].

Imaging of activity of caspase 3 through measurement of FRET between MiCy and mKO

The normalized excitation and emission spectra of MiCy and mKO (Figure 5A) demonstrate good overlap between the MiCy emission and the mKO excitation spectra, suggesting that the combination of MiCy and mKO may make a good donor/acceptor

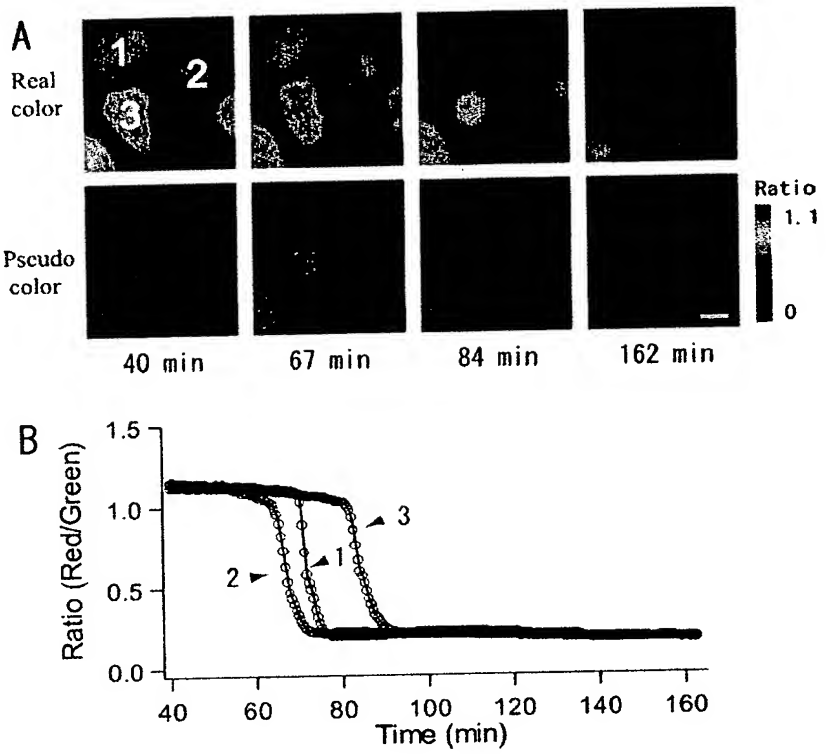

Figure 6 FRET imaging of caspase 3 activity during an apoptotic process

(**A**) FRET images of HeLa cells displayed in real colour and pseudo colour (ratios). Scale bar, 20 μM. (**B**) Time courses of the 559/495 nm emission ratios observed in the three cells indicated in (**A**).

pair for FRET. Construction of the unimolecular fluorescent indicator, encoded by a single gene, principally requires that either the donor or acceptor FP be monomeric. Thus we did not disrupt the ability of MiCy to dimerize; we linked the C-terminus of MiCy and the N-terminus of mKO using a peptide containing the caspase 3 cleavage sequence, DEVD (Asp-Glu-Val-Asp) (Figure 5C) [13,14]. The recombinant protein, prepared in bacteria, was examined using an excitation wavelength of 440 nm. FRET was observed as a decrease in the emission peak at 495 nm and an increase in the peak at 559 nm. Incubation of the sample with an activated recombinant caspase 3 (3.7 μg/ml) at 30 °C for 120 min completely abolished the FRET signal. The change in colour before and after treatment with caspase 3 was easily recognizable by eye as seen using a common digital camera through a Wratten film passing light of longer than 480 nm with excitation at 440 nm (Figure 5D, inset). The emission ratio of 559/495 nm decreased 14-fold. Neither caspase 8 nor caspase 9 altered the emission spectrum (results not shown). Therefore the chimaeric MiCy–mKO protein functions as a specific sensor for caspase 3 activity, despite dimerization of MiCy. After expressing this caspase-3-sensor protein in HeLa cells, we detected the two signals from MiCy and mKO simultaneously using a colour CCD camera containing three CCD chips (Figure 6). Following a 1.5-h exposure to 500 ng/ml anti-Fas antibody (CH-11) and 10 μg/ml cycloheximide at 37 °C, the value of the 559/495 emission ratio dropped progressively from 1.2 to 0.2 just before the shrinking of cells characteristic of apoptosis.

For broader FRET applications, any oligomerization induced through the fusion of an oligomerizing donor or acceptor FP is problematic. The engineering of a completely monomeric MiCy variant is now under way.

pH-sensitivity of FRET pairs: MiCy/mKO compared with CFP/YFP

Multiple critical cellular organelles, such as lysosomes, have extreme pHs. Even within the cytosol, alkalinization and acidification may occur during metabolic stress or mitogenic stimulation. Thus FP resistance to pH fluctuation is often required for effective quantitative imaging. To use FRET in studies of environments with extreme pHs, both the donor quantum yield and the acceptor molar absorption coefficient must be indifferent to changes in pH [15]. While most GFP-based FRET experiments use CFP and YFP as FRET donors and acceptors, CFP has an acid-sensitive quantum yield and YFP has an acid-sensitive molar absorption coefficient [15]. When pH decreases, these two negative effects reinforce each other, resulting in loss of FRET. Below pH 6.5, FRET from CFP to YFP is significantly disturbed. Therefore development of alternative donor/acceptor pairs has been greatly desired for more effective quantitative FRET imaging.

The lower pH-sensitivity of the mKO molar absorption coefficient than pH-insensitive variants of YFP, such as EYFP.1 (enhanced YFP; apparent $pK_a = 5.9$) [15], citrine (apparent $pK_a = 5.7$) [16] and Venus (apparent $pK_a = 6.0$), makes this

protein a desirable acceptor [17]. MiCy appears to be an ideal donor due to its pH-resistant quantum yield. While pH-sensitivity of the donor molar absorption coefficient is not important for pH-resistant FRET, a pH-resistant acceptor quantum yield would be preferable, because it facilitates the measurement of FRET efficiency by observing the ratio of donor to acceptor emissions. Again, mKO appears to make an ideal acceptor, as its quantum yield is completely indifferent to pH changes.

Optical factors for FRET measurements using MiCy/mKO compared with CFP/YFP

We compared the MiCy/mKO pair of excitation and emission spectra to that for CFP and YFP (Figure 5B). The MiCy/mKO pair appears to be free of the problems of the cross-excitation of acceptor and the cross-detection of the donor and FRET signals experienced with the CFP/YFP pair. Selective excitation of MiCy over mKO can be achieved using a 440AF21 (440 ± 10.5 nm) bandpass filter. As emission spectra often rise steeply and fall gradually as a function of wavelength, the donor emission can often spill over into the FRET channel. Such cross-detection is prominent for the CFP/YFP pair [18]. In contrast, the emissions of MiCy and mKO should be easily separable using appropriate bandpass filters. Also, the good spectral overlap between MiCy emission and mKO absorption and the high fluorescence quantum yield of MiCy creates a Förster's distance for the MiCy/mKO pair as large as 5.3 nm, while the value for CFP/YFP is 4.9 nm [19]. Together, these advantages of the MiCy/mKO pair may be responsible for the relatively large changes in FRET signals observed as a measure of caspase 3 activity.

We thank Dr Kenji Iwao and Dr Saburo Hosaka at Akajima Marine Science Laboratory for acquiring stony coral animals, Dr Isogai for assistance with analytical centrifugation, and Dr H. Watanabe and Dr M. Watanabe for lifetime fluorescence measurements. This work was partly supported by grants from CREST of JST (Japan Science and Technology), the Special Coordination Fund for the promotion of Ministry of Education, Culture, Sports, Science and Technology, the Japanese Government, NEDO (the New Energy and Industrial Technology Development Organization) and HFSP (Human Frontier Science Program).

REFERENCES

1 Tsien, R. Y. (1998) The green fluorescent protein. Annu. Rev. Biochem. **67**, 509–544
2 Matz, M. V., Fradokov, A. F., Labas, Y. A., Savitsky, A. P., Zaraisky, A. G., Markelov, M. L. and Lukyanov, S. A. (1999) Fluorescent proteins from nonbioluminescent Anthozoa species. Nat. Biotechnol. **17**, 969–973
3 Labas, Y. A., Gurskaya, N. G., Yanushevich, Y. G., Fradkov, A. F., Lukyanov, K. A., Lukyanov, S. A. and Matz, M. V. (2002) Diversity and evolution of the green fluorescent protein family. Proc. Natl. Acad. Sci. U.S.A. **99**, 4256–4261
4 Miyawaki, A. (2002) Green fluorescent protein-like proteins in reef Anthozoa animals. Cell Struct. Funct. **27**, 343–347
5 Chomczynski, P. and Sacchi, N. (1987) Single-step method of RNA isolation by acid guanidinium thiocyanate–phenol–chloroform extraction. Anal. Biochem. **162**, 156–159
6 Sawano, A. and Miyawaki, A. (2000) Directed evolution of green fluorescent protein by a new versatile PCR strategy for site-directed and semi-random mutagenesis. Nucleic Acids Res. **28**, E78
7 Nagai, T., Sawano, A., Park, E. S. and Miyawaki, A. (2001) Circularly permuted green fluorescent proteins engineered to sense Ca^{2+}. Proc. Natl. Acad. Sci. U.S.A. **98**, 3197–3202
8 Baird, G. S., Zacharias, D. A. and Tsien, R. Y. (2000) Biochemistry, mutagenesis, and oligomerization of DsRed, a red fluorescent protein from coral. Proc. Natl. Acad. Sci. U.S.A. **99**, 11984–11989
9 Ward, W. W. and Cormier, M. J. (1979) An energy transfer protein in coelenterate bioluminescence: Characterization of the *Renilla* green-fluorescent protein (GFP). J. Biol. Chem. **254**, 781–788
10 Tsurui, H., Nishimura, H., Hattori, S., Hirose, S., Okumura, K. and Shirai, T. (2000) Seven-color fluorescence imaging of tissue samples based on Fourier spectroscopy and singular value decomposition. J. Histochem. Cytochem. **48**, 653–662
11 Campbell, R. E., Tour, O., Palmer, A. E., Steinbach, P. A., Baird, G. S., Zacharias, D. A. and Tsien, R. Y. (2002) A monomeric red fluorescent protein. Proc. Natl. Acad. Sci. U.S.A. **99**, 7877–7882
12 Karasawa, S., Araki, T., Yamamoto-Hino, M. and Miyawaki, A. (2003) A green-emitting fluorescent protein from Galaxeidae coral and its monomeric version for use in fluorescent labeling. J. Biol. Chem. **278**, 34167–34171
13 Tyas, L., Brophy, V. A., Pope, A., Rivett, A. J. and Tavaré, J. M. (2000) Rapid caspase-3 activation during apoptosis revealed using fluorescence-resonance energy transfer. EMBO Rep. **1**, 266–270
14 Takemoto, K., Nagai, T., Miyawaki, A. and Miura, M. (2003) Spatio-temporal activation of caspase revealed by indicator that is insensitive to environmental effects. J. Cell Biol. **160**, 235–243
15 Miyawaki, A. and Tsien, R. Y. (2000) Monitoring protein conformations and interactions by fluorescence resonance energy transfer between mutants of green fluorescent protein. Methods Enzymol. **327**, 472–500
16 Griesbeck, O., Baird, G. S., Campbell, R. E., Zacharias, D. A. and Tsien, R. Y. (2001) Reducing the environmental sensitivity of yellow fluorescent protein: mechanism and applications. J. Biol. Chem. **276**, 29188–29194
17 Nagai, T., Ibata, K., Park, E. S., Kubota, M., Mikoshiba, K. and Miyawaki, A. (2002) A variant of yellow fluorescent protein with fast and efficient maturation for cell-biological applications. Nat. Biotechnol. **20**, 87–90
18 Erickson, M. G., Moon, D. L. and Yue, D. T. (2003) DsRed as a potential FRET partner with CFP and GFP. Biophys. J. **85**, 599–611
19 Patterson, G. H., Piston, D. W. and Barisas, B. G. (2000) Förster distances between green fluorescent protein pairs. Anal. Biochem. **284**, 438–440
20 Yang, F., Moss, L. G. and Phillips, Jr, G. N. (1996) The molecular structure of green fluorescent protein. Nat. Biotechnol. **14**, 1246–1251

Received 1 March 2004/31 March 2004; accepted 5 April 2004
Published as BJ Immediate Publication 5 April 2004, DOI 10.1042/BJ20040321